JCI The Journal of Clinical Investigation

# The vimentin intermediate filament network restrains regulatory T cell suppression of graft-versus-host disease

Cameron McDonald-Hyman, … , Michael L. Dustin, Bruce R. Blazar

*J Clin Invest.* 2018;128(10):4604-4621. https://doi.org/10.1172/JCI95713.

Research Article | Immunology | Transplantation

## Graphical abstract

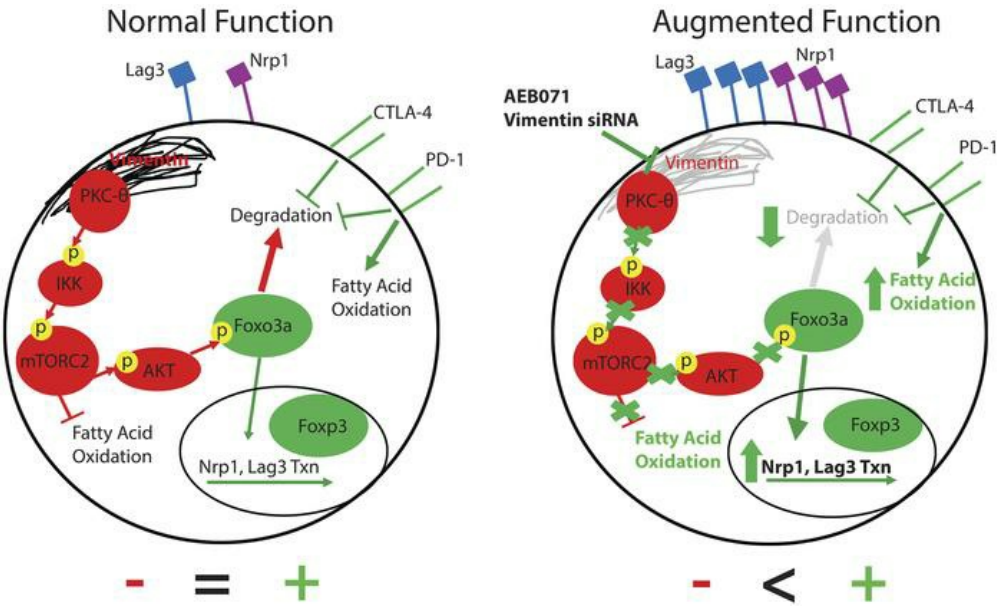

# The vimentin intermediate filament network restrains regulatory T cell suppression of graft-versus-host disease

Cameron McDonald-Hyman,[1,2] James T. Muller,[3] Michael Loschi,[1,2] Govindarajan Thangavelu,[1,2] Asim Saha,[1,2] Sudha Kumari,[3] Dawn K. Reichenbach,[1,2] Michelle J. Smith,[1,2] Guoan Zhang,[3] Brent H. Koehn,[1,2] Jiqiang Lin,[3] Jason S. Mitchell,[2,4] Brian T. Fife,[2,4] Angela Panoskaltsis-Mortari,[1] Colby J. Feser,[1] Andrew Kemal Kirchmeier,[1] Mark J. Osborn,[1] Keli L. Hippen,[1] Ameeta Kelekar,[5] Jonathan S. Serody,[6] Laurence A. Turka,[7] David H. Munn,[8] Hongbo Chi,[9] Thomas A. Neubert,[3] Michael L. Dustin,[10] and Bruce R. Blazar[1,2]

[1]Division of Blood and Marrow Transplantation, Department of Pediatrics, Masonic Cancer Center, University of Minnesota, Minneapolis, Minnesota, USA. [2]The Center for Immunology, University of Minnesota Medical School, Minneapolis, Minnesota, USA. [3]Skirball Institute of Biomolecular Medicine, and Department of Cell Biology, NYU School of Medicine, New York, New York, USA. [4]Division of Rheumatology, Department of Medicine, University of Minnesota Medical School, Minneapolis, Minnesota, USA. [5]Department of Laboratory Medicine and Pathology, University of Minnesota, Minneapolis, Minnesota, USA. [6]Lineberger Comprehensive Cancer Center, Division of Hematology/Oncology, University of North Carolina, Chapel Hill, North Carolina, USA. [7]Center for Transplantation Sciences, Department of Surgery, Massachusetts General Hospital, Boston, Massachusetts, USA. [8]Department of Pediatrics, Georgia Health Sciences University, Augusta, Georgia, USA. [9]Department of Immunology, Saint Jude Children's Research Hospital, Memphis, Tennessee, USA. [10]Kennedy Institute of Rheumatology, Nuffield Department of Orthopaedics, Rheumatology and Musculoskeletal Sciences, University of Oxford, Oxford, United Kingdom.

**Regulatory T cells (Tregs) are critical for maintaining immune homeostasis. However, current Treg immunotherapies do not optimally treat inflammatory diseases in patients. Understanding the cellular processes that control Treg function may allow for the augmentation of therapeutic efficacy. In contrast to activated conventional T cells, in which protein kinase C-θ (PKC-θ) localizes to the contact point between T cells and antigen-presenting cells, in human and mouse Tregs, PKC-θ localizes to the opposite end of the cell in the distal pole complex (DPC). Here, using a phosphoproteomic screen, we identified the intermediate filament vimentin as a PKC-θ phospho target and show that vimentin forms a DPC superstructure on which PKC-θ accumulates. Treatment of mouse Tregs with either a clinically relevant PKC-θ inhibitor or vimentin siRNA disrupted vimentin and enhanced Treg metabolic and suppressive activity. Moreover, vimentin-disrupted mouse Tregs were significantly better than controls at suppressing alloreactive T cell priming in graft-versus-host disease (GVHD) and GVHD lethality, using a complete MHC-mismatch mouse model of acute GVHD (C57BL/6 donor into BALB/c host). Interestingly, vimentin disruption augmented the suppressor function of PKC-θ–deficient mouse Tregs. This suggests that enhanced Treg activity after PKC-θ inhibition is secondary to effects on vimentin, not just PKC-θ kinase activity inhibition. Our data demonstrate that vimentin is a key metabolic and functional controller of Treg activity and provide proof of principle that disruption of vimentin is a feasible, translationally relevant method to enhance Treg potency.**

## Introduction

Regulatory T cells (Tregs) are critical for maintaining immune homeostasis and preventing autoimmune and inflammatory disorders (1, 2). However, they also support cancer progression by suppressing antitumor immunity (3). Therapeutic approaches to enhance Treg development and function by pharmacologic agents such as metabolic inhibitors or by direct administration of Tregs are often effective in treating autoimmune and inflammatory diseases in mice (4), but are less so in the clinic. For example, Treg cellular therapy is not uniformly efficacious in preventing or treating graft-versus-host disease (GVHD), the primary cause of morbidity and mortality after allogeneic hematopoietic stem cell transplantation (5–8). In the setting of cancer, a variety of strategies to modulate Treg function and abundance in the tumor microenvironment have been tested, although successful treatments have resulted in autoimmune diseases in some settings (9, 10). Thus, a greater depth of understanding of Treg biology is needed to overcome our current limitations in effectively altering Treg activity to treat disease.

When T cells form a productive contact with an antigen-presenting cell (APC), an immunological synapse (IS) forms (11). This IS provides the spatial organization of signaling molecules that initiate and sustain T cell activation. In addition, T cell–APC binding catalyzes the formation of a T cell distal pole complex (DPC), a structure that has been postulated to be important for the sorting of negative regulatory proteins away from the IS (12). We previously showed that, while protein kinase C-θ (PKC-θ) localizes to the IS in conventional T cells (Tcons), PKC-θ, by contrast, localizes to the DPC in Tregs (13). This finding has now

**Authorship note:** CMH and JTM are co–first authors. ML and GT, as well as MLD and BRB, contributed equally to this work.
**Conflict of interest:** The authors have declared that no conflict of interest exists.
**Submitted:** June 14, 2017; **Accepted:** July 26, 2018.
**Reference information:** *J Clin Invest*. 2018;128(10):4604–4621.
https://doi.org/10.1172/JCI95713.

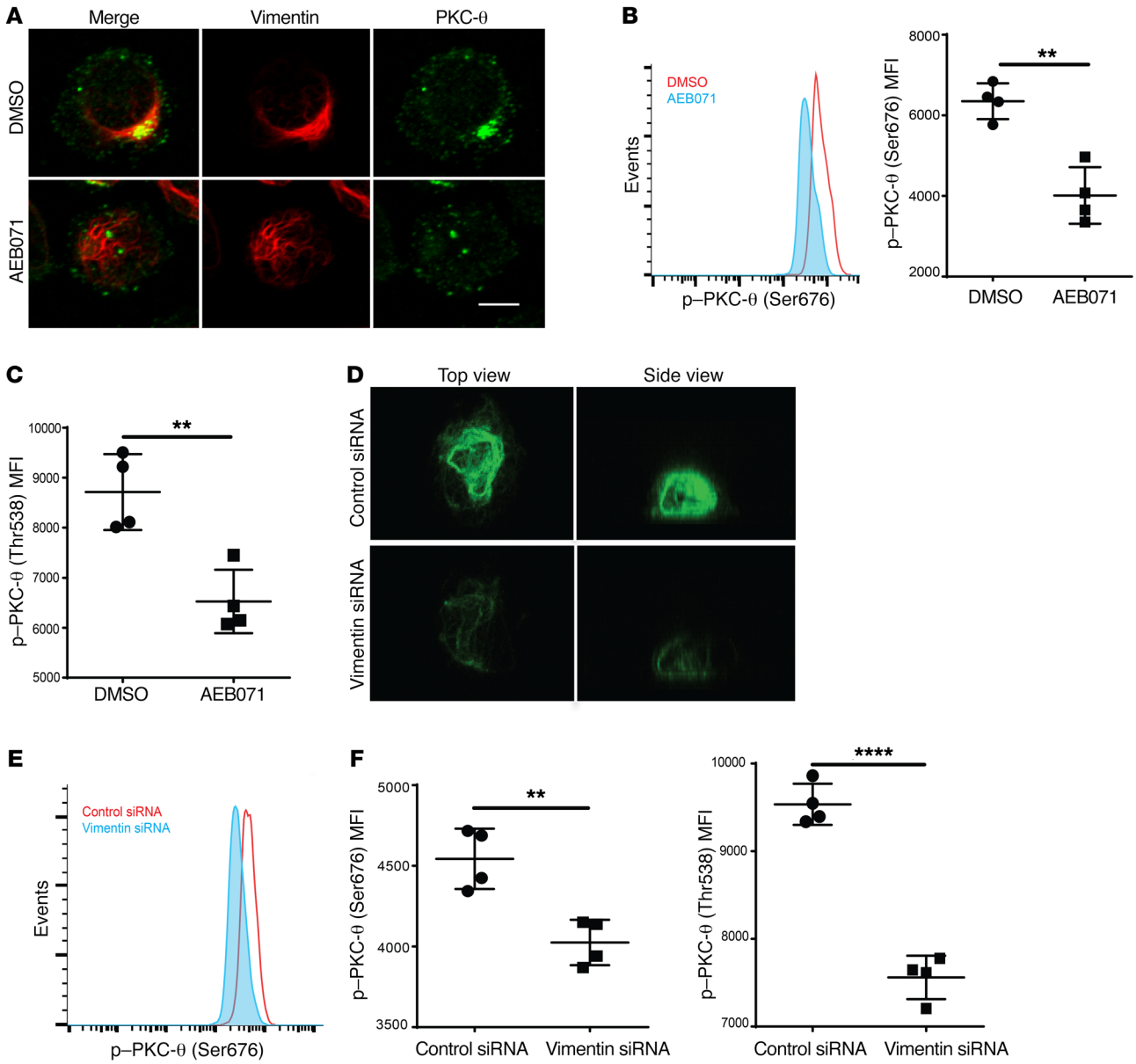


**Figure 1. Vimentin superstructure is disrupted by PKC-θ or vimentin inhibition.** (**A**) Confocal microscopic images of PKC-θ and vimentin in activated Tregs pretreated with DMSO or AEB071. Scale bar: 5 μm. (**B** and **C**) Phosphoflow of PKC-θ autophosphorylation at (**B**) Ser676 and (**C**) Thr538 in activated Tregs pretreated with DMSO or AEB071. (**D**) Confocal microscopic images of vimentin staining in Tregs transfected with control or vimentin siRNA. Original magnification, ×43. (**E** and **F**) Phosphoflow of PKC-θ autophosphorylation at (**E**) Ser676 and (**F**) Thr538 in activated Tregs pretreated with control or vimentin siRNA. Data show 1 representative experiment of 4 (**A**), or 3 (**B**–**F**) independent experiments. $n = 4$ replicates/group (**B**, **C**, **E**, and **F**). $^{**}P < 0.01$ and $^{****}P < 0.0001$, by unpaired Student's $t$ test. MFI, median fluorescence intensity. Error bars indicate the SEM.

been confirmed by another group (14). Moreover, pharmacologic inhibition of PKC-θ both disrupts the Treg DPC and augments human and WT murine Treg suppression (13, 15). Paradoxically, however, PKC-θ–KO murine Tregs are not functionally enhanced (16), suggesting a more complex role of PKC-θ inhibition beyond its kinase targeting function.

To address how PKC-θ inhibition promotes Treg activity and to identify novel targets to augment Treg function, we performed a phosphoproteomic screen to search for PKC-θ phospho-targets, which revealed that phosphorylation of the cytoskeletal protein vimentin was downregulated by PKC-θ inhibition. Importantly, we found that PKC-θ cobound with vimentin on a large vimentin superstructure at the Treg DPC and observed that PKC-θ inhibitor treatment and vimentin knockdown each disrupted vimentin at the DPC and markedly augmented Treg suppressor function and oxidative metabolism. Last, Treg adoptive transfer of vimentin-disrupted Tregs proved to be significantly more potent than were control-treated Tregs in suppressing GVHD lethality. Our findings support a model by which the DPC plays an important role in the negative regulation of Treg function and identify vimentin as a new modulator of Treg activation. Thus, these studies identify a key link between the DPC, the cytoskeleton, and intracellular signaling that

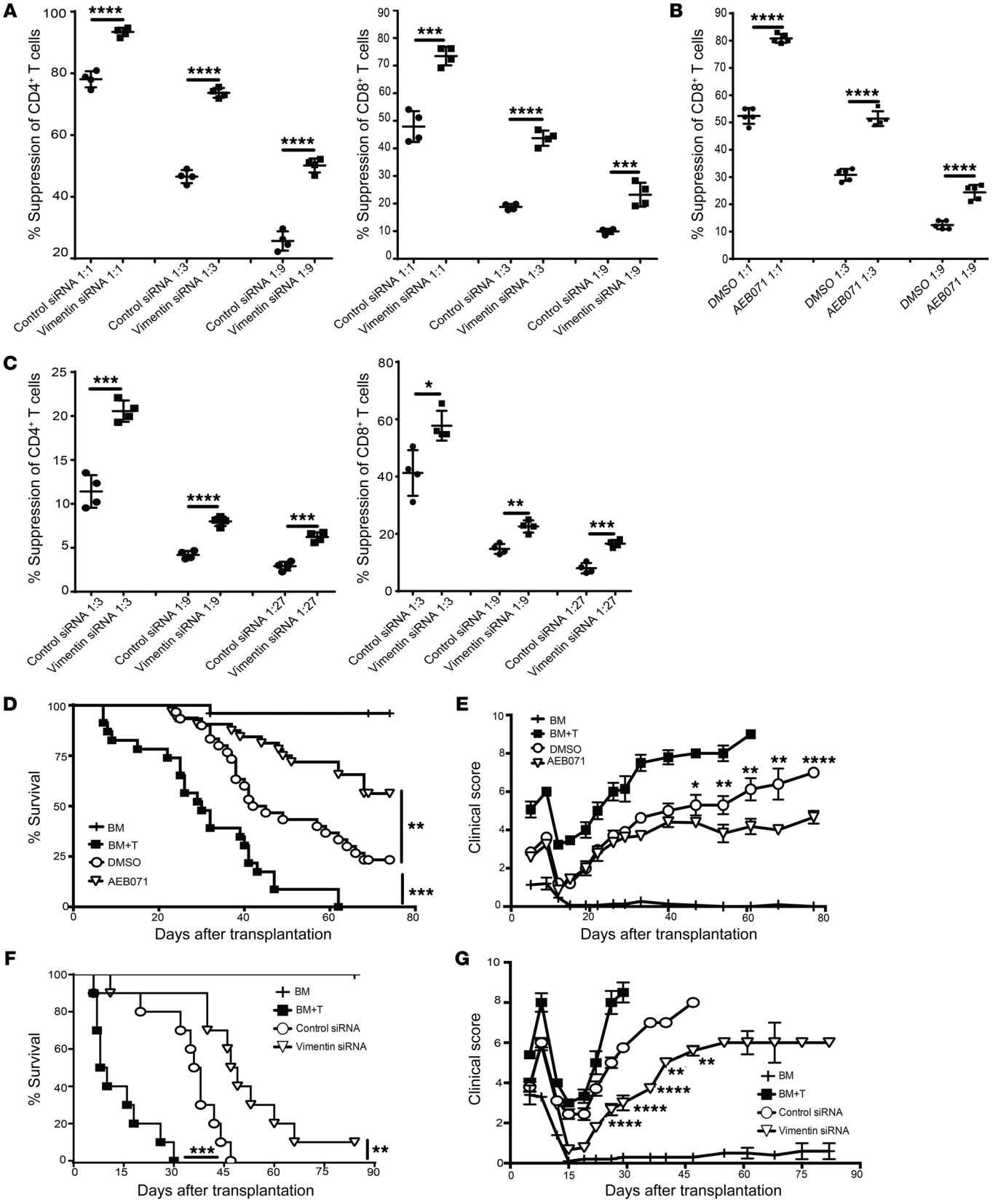
A
% Suppression of CD4+ T cells
% Suppression of CD8+ T cells
Control siRNA 1:1
Vimentin siRNA 1:1
Control siRNA 1:3
Vimentin siRNA 1:3
Control siRNA 1:9
Vimentin siRNA 1:9
B
% Suppression of CD8+ T cells
DMSO 1:1
AEB071 1:1
DMSO 1:3
AEB071 1:3
DMSO 1:9
AEB071 1:9
C
% Suppression of CD4+ T cells
% Suppression of CD8+ T cells
Control siRNA 1:3
Vimentin siRNA 1:3
Control siRNA 1:9
Vimentin siRNA 1:9
Control siRNA 1:27
Vimentin siRNA 1:27
D
% Survival
BM
BM+T
DMSO
AEB071
Days after transplantation
E
Clinical score
BM
BM+T
DMSO
AEB071
Days after transplantation
F
% Survival
BM
BM+T
Control siRNA
Vimentin siRNA
Days after transplantation
G
Clinical score
BM
BM+T
Control siRNA
Vimentin siRNA
Days after transplantation

**Figure 2. Vimentin disruption augments Treg function.** (**A**–**C**) Suppression of (**A**) $CD4^+$ and $CD8^+$ Tcon proliferation by WT Tregs transfected with control or vimentin siRNA, (**B**) $CD8^+$ Tcon proliferation by DMSO- or AEB071-pretreated WT Tregs, and (**C**) $CD4^+$ and $CD8^+$ Tcon proliferation by PKC-θ–KO Tregs transfected with either control or vimentin siRNA in classical in vitro Treg suppression assays. 1:1 to 1:9 Treg/Tcon ratio. (**D**) Survival and (**E**) clinical GVHD scores (0 = no disease, 10 = severe disease) for recipient mice after receiving BM, BM plus Tcons (BM+T), or BM plus Tcons plus Tregs pretreated with DMSO or AEB071 (DMSO or AEB071). Data were pooled from 4 independent experiments. BM, $n = 25$; BM+T, $n = 29$; DMSO, $n = 29$; AEB071, $n = 31$. (**F**) Survival and (**G**) clinical GVHD scores for recipient mice after receiving BM only, BM plus Tcons, or BM plus Tcons plus Tregs transfected with control or vimentin siRNA. Data were pooled from 2 independent experiments. BM, $n = 10$; BM plus Tcons, $n = 12$; control siRNA, $n = 12$; vimentin siRNA, $n = 12$. Statistical comparisons in **E** and **G** represent DMSO versus AEB071 and control versus vimentin siRNA, respectively. Data in **A**–**C** are results from 1 representative experiment of 4 independent experiments. $^*P < 0.05$, $^{**}P < 0.01$, $^{***}P < 0.001$, and $^{****}P < 0.0001$, by 1-way ANOVA with multiple comparisons analysis and Tukey's post test (**A**–**C**), log-rank test for survival analysis (**D** and **F**), and unpaired Student's *t* test (**E** and **G**). Error bars indicate the SEM.

is critical for supporting Tcon function but that, in contrast, serves to restrain Treg suppressor function. These studies also demonstrate proof of principle that disrupting vimentin is a feasible and translationally relevant method to enhance Treg therapy.

## Results

*PKC-θ and vimentin complex at the Treg DPC*. Our previous work demonstrated that PKC-θ inhibition in Tregs with compound 20 (C20), a highly specific but nontranslationally relevant small-molecule PKC-θ inhibitor (13), leads not only to augmented Treg suppressor function but also to DPC disruption, suggesting a role for the DPC in modulated Treg function. Therefore, we first examined PKC-θ at the DPC to better understand the relationship between these structures. As observed previously (13), localization of PKC-θ to the DPC is directly augmented by exposure of Tregs to Ab-coated (CD4- or CD25-coated) nanoparticles (Supplemental Figure 1, A and B; supplemental material available online with this article; https://doi.org/10.1172/JCI95713DS1), which enhanced our ability to image these structures. Super-resolution imaging of the DPC revealed that the DPC was composed of PKC-θ foci that were associated with a dense network of vimentin filaments (Figure 1A and Supplemental Figure 1B). A brief 30-minute treatment with the clinically tested PKC-θ inhibitor AEB071 both disrupted recruitment of PKC-θ foci to the vimentin superstructure and disassociated vimentin filaments (Figure 1A), suggesting a regulated interaction between PKC-θ and vimentin at the DPC. To obtain independent confirmation of the relationship between PKC-θ and vimentin, we performed an unbiased stable isotope labeling with amino acids in cell culture (SILAC) phosphoproteomic screen (17) of consensus PKC-θ phosphorylation sites in activated human Tregs pretreated with either DMSO or AEB071. We found that AEB071 treatment significantly reduced vimentin phosphorylation, along with the phosphorylation of 68 other proteins (Supplemental Table 1). Phosphoflow analysis further demonstrated that AEB071 treatment reduced auto- and transphosphorylation of PKC-θ (Figure 1, B and C), both of which are critical for complete PKC-θ activation (18).

In addition to the interaction between PKC-θ and vimentin, we also noted that the Tregs contained substantially higher levels of vimentin than did $CD4^+$ Tcons (Supplemental Figure 1C). Therefore, we asked whether knockdown of vimentin would modify the vimentin network at the DPC in a manner similar to AEB071 treatment, and, secondarily, reduce PKC-θ activity. Indeed, we found that siRNA-mediated knockdown of vimentin by as little as 31% (Supplemental Figure 1D; range 31%–73%) changed the vimentin superstructure from a densely interwoven basket to a sparse filament network (Figure 1D). In WT Tregs, vimentin siRNA also reduced PKC-θ auto- and transphosphorylation (Figure 1, E and F), indicating that vimentin supports PKC-θ activity. Importantly, the effects of vimentin knockdown did not require PKC-θ. PKC-θ–KO Tregs formed identical vimentin superstructures after activation, and treatment with vimentin siRNA disrupted the vimentin network in a manner similar to that seen with WT Tregs (Supplemental Figure 2A). These results suggest that vimentin is a key element of the Treg DPC and that, while PKC-θ localizes to the DPC, it may not be a necessary DPC component with respect to the modulation of Treg suppression.

*Vimentin disruption augments Treg suppression, leading to increased GVHD therapeutic efficacy*. To further explore the role of vimentin in Tregs, we assessed the functional consequences of disrupting the vimentin superstructure. Both vimentin knockdown and AEB071 pretreatment enhanced Treg suppression in standard, contact-dependent in vitro Treg suppression assays (ref. 19; Figure 2, A and B, and Supplemental Figure 2B). Treatment of vimentin siRNA–transfected Tregs with AEB071 did not significantly augment Treg function above that observed with vimentin siRNA transfection alone (Supplemental Figure 2C). Notably, the effect of AEB071 on Treg function was nearly identical to that of the highly PKC-θ–specific inhibitor C20 (Supplemental Figure 2D). Given our structural findings in PKC-θ–KO Tregs, we hypothesized that the vimentin network, even in the absence of PKC-θ, might limit the suppressive capacity of Tregs. Consistent with this, siRNA-mediated vimentin disruption augmented both PKC-θ-KO and WT Treg function (Figure 2C), further supporting the idea of a PKC-θ–independent role for vimentin.

As Treg infusions have been tested in clinical trials for GVHD prevention (20, 21), we used a fully MHC-disparate GVHD model (22) to assess the function of donor Tregs, in which vimentin had been disrupted using AEB071 pretreatment or vimentin siRNA. Compared with controls, adoptive transfer of AEB071-pretreated or vimentin-knockdown Tregs significantly improved recipient survival, GVHD clinical scores, and weights (Figure 2, D–G, and Supplemental Figure 2, E and F), indicating enhanced GVHD suppression. Neither AEB071 nor vimentin siRNA altered Treg homing to the gastrointestinal (GI) tract, the primary site for GVHD-induced lethality (23), based on GI homing molecule expression (Supplemental Figure 3, A and B) and Treg numbers in the GI tract (Supplemental Figure 3C), nor did they alter overall Treg numbers, persistence, or localization after transplantation as assessed by bioluminescence imaging (BLI) over time using luciferase-transgenic Tregs (Supplemental Figure 3, D and F). Together, these data suggest that vimentin disruption augments Treg function in vitro and in vivo, without altering Treg survival or homing.

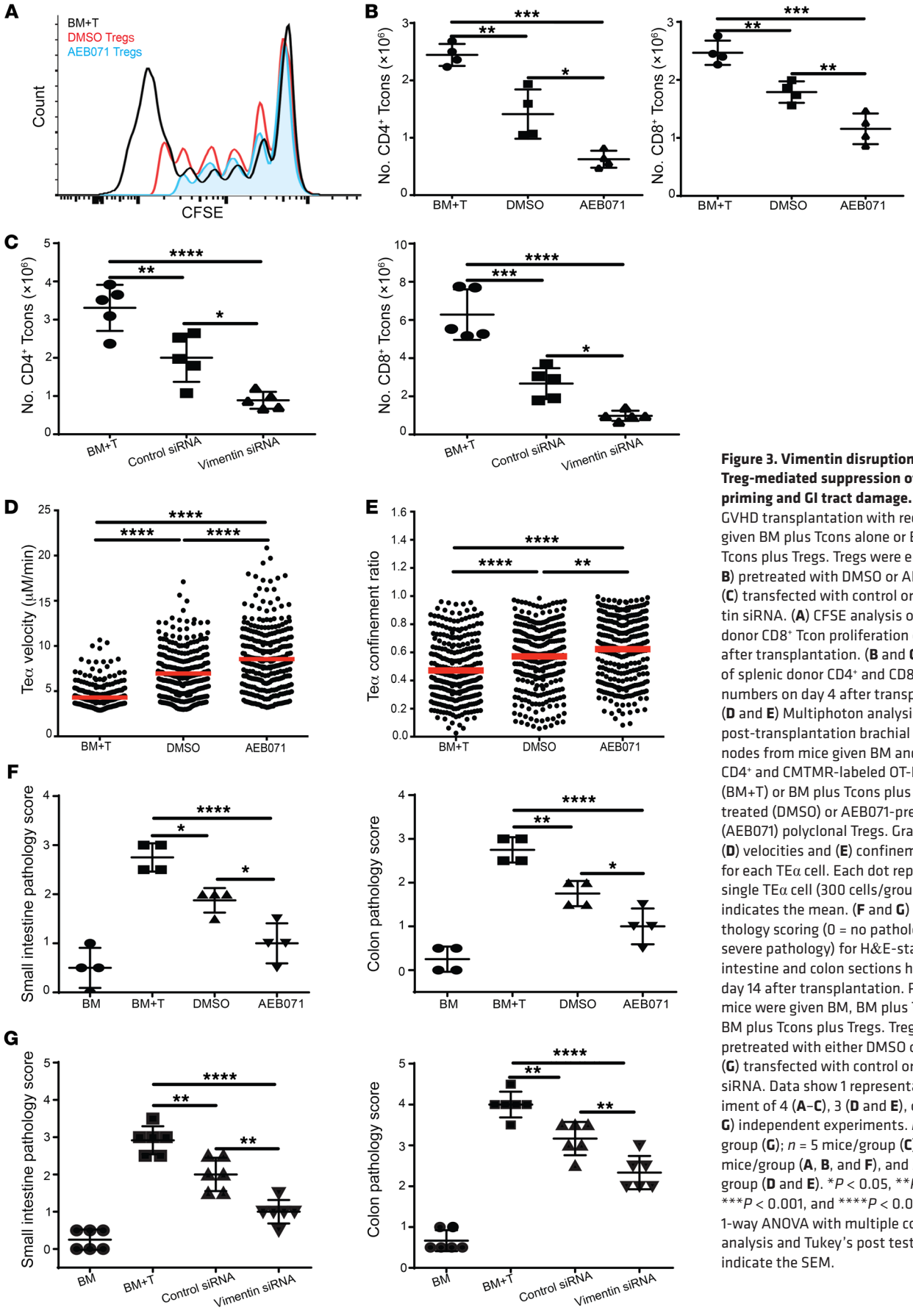


**Figure 3. Vimentin disruption increases Treg-mediated suppression of Tcon priming and GI tract damage.** (**A**–**C**) GVHD transplantation with recipient mice given BM plus Tcons alone or BM plus Tcons plus Tregs. Tregs were either (**A** and **B**) pretreated with DMSO or AEB071 or (**C**) transfected with control or vimentin siRNA. (**A**) CFSE analysis of splenic donor CD8$^+$ Tcon proliferation on day 4 after transplantation. (**B** and **C**) Analysis of splenic donor CD4$^+$ and CD8$^+$ Tcon numbers on day 4 after transplantation. (**D** and **E**) Multiphoton analysis of day-4 post-transplantation brachial lymph nodes from mice given BM and EGFP-TEα CD4$^+$ and CMTMR-labeled OT-I CD8$^+$ alone (BM+T) or BM plus Tcons plus DMSO-pretreated (DMSO) or AEB071-pretreated (AEB071) polyclonal Tregs. Graphs show (**D**) velocities and (**E**) confinement ratios for each TEα cell. Each dot represents a single TEα cell (300 cells/group). Red line indicates the mean. (**F** and **G**) Histopathology scoring (0 = no pathology, 4 = severe pathology) for H&E-stained small intestine and colon sections harvested on day 14 after transplantation. Recipient mice were given BM, BM plus Tcons, or BM plus Tcons plus Tregs. Tregs were (**F**) pretreated with either DMSO or AEB071 or (**G**) transfected with control or vimentin siRNA. Data show 1 representative experiment of 4 (**A**–**C**), 3 (**D** and **E**), or 2 (**F** and **G**) independent experiments. $n$ = 6 mice/group (**G**); $n$ = 5 mice/group (**C**), $n$ = 4 mice/group (**A**, **B**, and **F**), and $n$ = 3 mice/group (**D** and **E**). *$P < 0.05$, **$P < 0.01$, ***$P < 0.001$, and ****$P < 0.0001$, by 1-way ANOVA with multiple comparisons analysis and Tukey's post test. Error bars indicate the SEM.

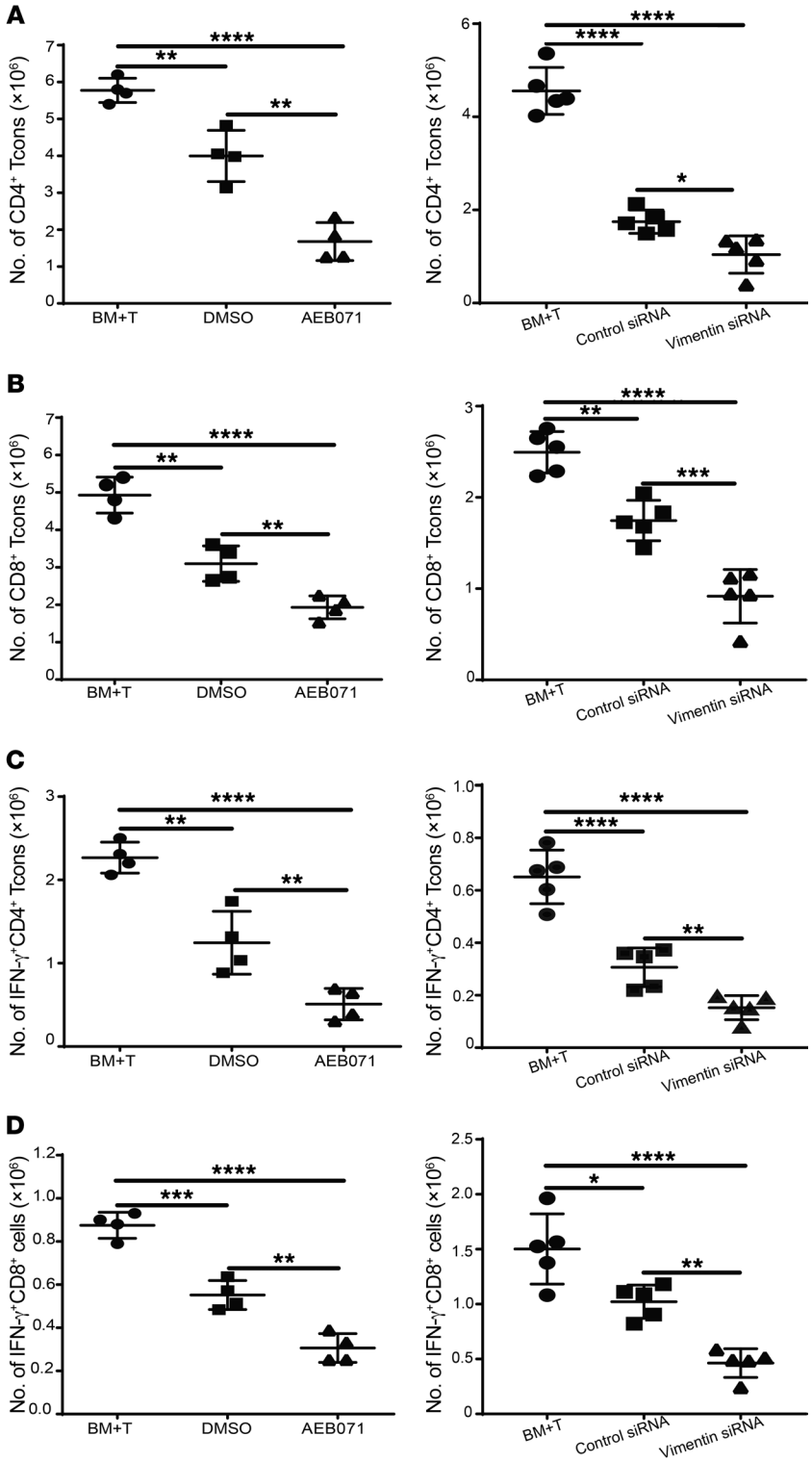


**Figure 4. Vimentin disruption increases Treg-mediated suppression of Tcon function in the GI tract.** (**A**–**D**) GVHD transplantation, with recipient mice given BM plus Tcons alone (BM+T) or BM plus Tcons plus Tregs. Tregs were pretreated with either DMSO or AEB071 or transfected with control or vimentin siRNA. Total number of (**A**) $CD4^+$ and (**B**) $CD8^+$ Tcons, along with the total number of (**C**) IFN-$\gamma^+CD4^+$ and (**D**) $CD8^+$ Tcons isolated from recipient mouse small intestine LP on day 14 after transplantation. Data from 1 of 3 independent experiments are shown. $n = 4$ mice/group for DMSO and AEB071 transplants; $n = 5$ mice/group for control and vimentin siRNA transplants. $^*P < 0.05$, $^{**}P < 0.01$, $^{***}P < 0.001$, and $^{****}P < 0.0001$, by 1-way ANOVA with multiple comparisons analysis and Tukey's post test. Error bars indicate the SEM.

*Vimentin-disrupted Tregs are superior in suppressing alloantigen-specific T cell priming in GVHD*. Since inhibition of Tcon priming is a critical Treg-suppressive mechanism (24), we hypothesized that augmented GVHD inhibition after vimentin disruption by AEB701 or vimentin siRNA may be due to enhanced suppression of Tcon activation. Consistent with this, we found reduced Tcon proliferation and numbers on day 4 after transplantation in mice given AEB071- or vimentin siRNA–pretreated Tregs (Figure 3, A–C). Direct examination of antigen-specific priming using multiphoton microscopy and a GVHD model with host alloantigen–specific Tcons ($CD4^+$ TEα), irrelevant Tcons ($CD8^+$ OT-I), and polyclonal Tregs showed that AEB071-pretreated Tregs reduced antigen-specific $CD4^+$ TE cell priming more than did controls (Figure 3, D and E; Supplemental Figure 4, A–F; and Supplemental Videos 1–6). Tregs had modest effects on OT-I, with no differences between Treg groups (Supplemental Figure 4, A–F, and Supplemental Videos 1–6). Furthermore, examination of the GI tract revealed a significant reduction in GVHD-related damage (Figure 3, F and G), as well as fewer total Tcons and fewer effector cytokine–producing Tcons in mice given AEB071- or vimentin siRNA–pretreated Tregs (Figure 4, A–D, and Supplemental Figure 4, G and H). In combination, our functional data suggest that vimentin supports signaling that restrains Treg function and that disrupting vimentin augments Treg potency in part by enhancing the suppression of Tcon antigen–specific priming and effector differentiation.

*Treg-suppressive cell-surface molecules are increased after vimentin disruption*. To characterize how alterations in the vimentin network augment Treg function, we assessed the expression of Treg-suppressive molecules. We detected no differences between controls and AEB071- pretreated or vimentin-knockdown Tregs in the expression of many molecules, including Foxp3, CTLA-4, and PD-1, or in the number of IL-10–producing Tregs in vivo (Supplemental Figure 5, A–C, not shown). However, both PKC-θ inhibition and vimentin knockdown increased neutropilin 1 (Nrp1) and lymphocyte-activating gene 3 (Lag3) expression (Figure 5, A–C), two molecules involved in Treg-mediated suppression of antigen-specific priming (24). Using standard, contact-dependent in vitro Treg suppression assays, in which Lag3 is functionally important (25), we found that Ab blockade of Lag3 significantly reduced the suppression of both AEB071- and vimentin siRNA–pretreated Tregs (Figure 5, D and E, and Supplemental Figure 5, D and E).

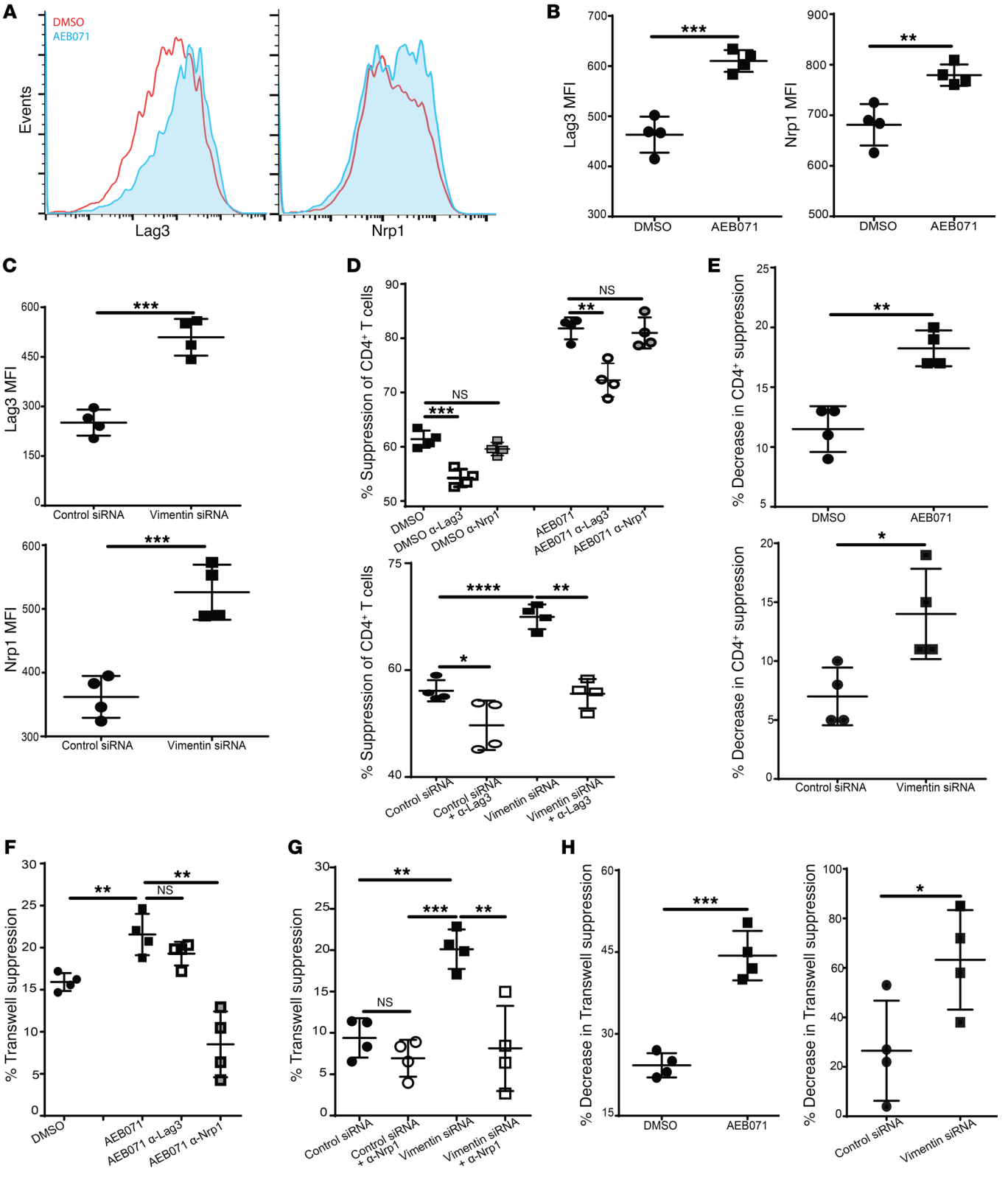
A
DMSO
AEB071
Events
Lag3
Nrp1
B
Lag3 MFI
Nrp1 MFI
DMSO
AEB071
C
Lag3 MFI
Nrp1 MFI
Control siRNA
Vimentin siRNA
D
% Suppression of CD4+ T cells
DMSO
DMSO α-Lag3
DMSO α-Nrp1
AEB071
AEB071 α-Lag3
AEB071 α-Nrp1
Control siRNA
Control siRNA + α-Lag3
Vimentin siRNA
Vimentin siRNA + α-Lag3
E
% Decrease in CD4+ suppression
F
% Transwell suppression
G
% Transwell suppression
Control siRNA + α-Nrp1
Vimentin siRNA + α-Nrp1
H
% Decrease in Transwell suppression

**Figure 5. Vimentin disruption increases Nrp1 and Lag3 expression.** (**A**–**C**) Analysis of Nrp1 and Lag3 expression on splenic donor Tregs on day 4 after GVHD transplantation, with recipient mice given BM plus Tcons plus Tregs. Mice were given either (**A** and **B**) DMSO- or AEB071-pretreated Tregs or (**C**) control or vimentin siRNA–transfected Tregs. (**D**) Suppression of $CD4^+$ Tcon proliferation by DMSO- and AEB071-pretreated or control and vimentin siRNA–pretreated Tregs in classical in vitro suppression assays with either isotype or anti-Lag3–blocking mAb (α-Lag3) or anti-Nrp1–blocking mAb (α-Nrp1). 1:3 Treg/Tcon ratio. (**E**) Quantifications of the percentage of reduction of suppression with the anti-Lag3 treatment shown in **D**. (**F** and **G**) Percentage of in vitro Transwell suppression of $CD4^+$ Tcon proliferation by (**F**) DMSO- or AEB071-pretreated Tregs or (**G**) control or vimentin siRNA–pretreated Tregs. Groups were given isotype, anti-Lag3–blocking mAb, or anti-Nrp1–blocking mAb. (**H**) Quantification of the percentage of reduction in Transwell suppression with the anti-Nrp1 treatment shown in **F** and **G**. Data for 1 representative experiment of 4 independent experiments are shown. $n = 4$ mice/group (**A**–**C**); $n = 4$ replicates/group (**D**–**H**). $^*P < 0.05$, $^{**}P < 0.01$, $^{***}P < 0.001$, and $^{****}P < 0.0001$, by unpaired Student's $t$ test (**B**, **C**, **E**, and **H**) and 1-way ANOVA with multiple comparisons analysis and Tukey's post test (**D**, **F**, and **G**). Error bars indicate the SEM.

Consistent with published data (19), Nrp1 blockade had no effect in this assay (Figure 5D, Supplemental Figure 5D, and not shown), and a combination of Abs was similar to the results seen with Lag3 alone (data not shown). To examine the functional importance of Nrp1, we used Transwell assays (19). We found that Nrp1 blockade significantly reduced the suppression of AEB071-pretreated and vimentin siRNA–pretreated Tregs (Figure 5, F and G). Suppression of DMSO-treated Tregs was reduced, but not as robustly as suppression of AEB071-pretreated Tregs (Figure 5H and Supplemental Figure 5F). Similarly, Nrp1 blockade in control siRNA–transfected Tregs had significantly less effect compared with vimentin siRNA–treated Tregs (Figure 5, G and H). Lag3 blockade had no effect (Figure 5F and Supplemental Figure 5F, not shown), consistent with the current model of Lag3-mediated Treg suppression (24). Together, these data demonstrate that disruption of vimentin augments Nrp1 and Lag3 expression, which may directly contribute to increased Treg function.

*Vimentin disruption reduces Treg mTORC2 function and augments their metabolic fitness in GVHD*. Expression of Nrp1 and Lag3 is driven by Foxo3a (19) (DECODE analysis, http://gnc-pro.sabiosciences.com), a transcription factor that promotes Treg function (26). Mammalian target of rapamycin complex 2 (mTORC2) reduces Foxo3a activity through phosphorylation-dependent nuclear exclusion (26), and PKC-θ may promote this process through IκB kinase (IKK) (26–28). Since vimentin supports PKC-θ function and vimentin disruption reduces PKC-θ activation, we hypothesized that augmented expression of Nrp1 and Lag3 may be due to reduced PKC-θ and mTORC2 activity. Phosphoflow analysis revealed significant reductions in phosphorylation downstream of mTORC2, including Foxo3a, after AEB071 treatment and vimentin knockdown (Figure 6, A–D). In contrast, we observed no differences in phosphorylation of mTORC1-dependent molecules or PI3K-mediated phosphorylation of AKT (Supplemental Figure 6, A–C), known to be required for Treg suppressor function (29). Furthermore, PKC-θ siRNA and IKK inhibition each reduced mTORC2-dependent phosphorylation, without affecting mTORC1 (Figure 6, E and F, and Supplemental Figure 6, D and E). In combination, these data indicate that disrupting the vimentin network results in reduced mTORC2 activity, including diminished Foxo3a phosphorylation, and that this may be due in part to decreased PKC-θ/IKK signaling.

mTOR signaling also plays a critical role in regulating Treg metabolism (30–32). Specifically, Tregs preferentially oxidize fatty acids (FAs) as fuel, and mTORC1 may promote this process (33, 34). However, unchecked mTORC2 signaling leads to an increase in glycolysis and reduced Treg function (30, 31). Therefore, we hypothesized that because vimentin disruption increased Treg function and reduced mTORC2 signaling, it may also alter Treg metabolic activity by increasing FA uptake or energy generation from FA metabolism. Consistent with this, AEB071 treatment and vimentin knockdown each increased Treg oxidative phosphorylation in vitro (Figure 7, A and B). In GVHD, both AEB071- and vimentin siRNA–pretreated Tregs in spleens on day 4 after transplantation had augmented expression of CPT1a, the rate-limiting enzyme in mitochondrial FA oxidation (33) and had increased FA uptake compared with controls (Figure 7, C and D, and Supplemental Figure 7, A and B). We also noted increased expression of nutrient receptors (Figure 7, E and F, and Supplemental Figure 7C), but no changes in glucose utilization (Supplemental Figure 7, D and E) or expression of the glucose transporter Glut1 (Supplemental Figure 7, F and G), or in mitochondrial membrane potential or mass (Supplemental Figure 7, H–K). AEB071- and vimentin siRNA–pretreated Tregs in the small intestine on day 14 after transplantation had an identical phenotype, including increased expression of nutrient receptor and CPT1a, as well as augmented FA uptake (Figure 7, G and H). Thus, increased suppression of GVHD by vimentin-disrupted Tregs was associated with increased Treg metabolic fitness, as denoted by increased FA uptake and oxidative metabolism, without changes in glycolysis.

Additionally, we hypothesized that increased Treg suppression and metabolic activity might alter Tcon metabolic fitness in GVHD. Indeed, both AEB071- and vimentin siRNA–pretreated Tregs reduced Tcon expression of nutrient receptors and Glut1 in the spleen (Figure 8, A and B) and small intestine (Figure 9, A and B). In the small intestine, Tcon CPT1a expression was also reduced (Figure 9, C and D). Since alloreactive effector Tcons in GVHD can preferentially utilize FAs for fuel (35), reduced CPT1a expression suggests diminished effector activity, a finding consistent with our data showing reduced priming and cytokine production. These data demonstrate that modulating vimentin integrity increases Treg metabolic activity, including specific augmentations in FA utilization pathways, and that this metabolic enhancement is associated with reduced Tcon metabolic fitness.

## Discussion

Although Tregs are intimately involved in the pathogenesis of autoimmune and inflammatory disorders as well as cancer progression, successfully manipulating Tregs to dampen these diseases has proven challenging. Here, we demonstrate a proof of concept that targeting vimentin may be a method to enhance Treg therapeutic efficacy by showing the superior potency of vimentin-disrupted Tregs in the suppression of GVHD lethality and alloantigen-specific Tcon priming and function. Furthermore, we found that the vimentin network acts as an independent regula-

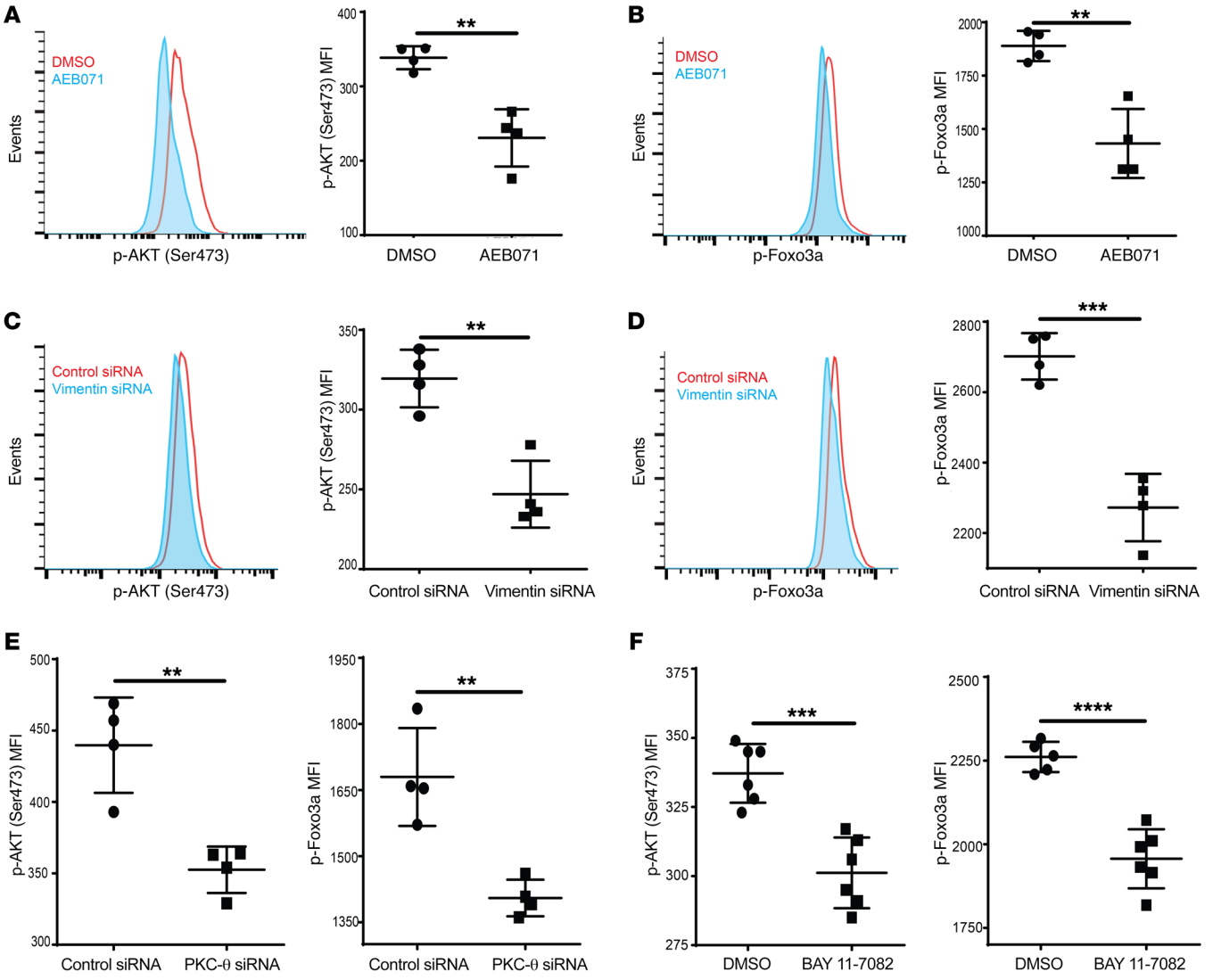


**Figure 6. Vimentin disruption reduces mTORC2 signaling.** (**A**–**F**) Phosphoflow analysis of mTORC2-downstream molecules p-AKT (Ser473) and p-Foxo3a in activated Tregs that were (**A** and **B**) pretreated with DMSO or AEB071, (**C** and **D**) transfected with control or vimentin siRNA, (**E**) transfected with control or PKC-θ siRNA, or (**F**) pretreated with DMSO or the IKK inhibitor BAY 11-7082. Data are from 1 representative experiment of 4 (**A**–**C**) or 2 (**E** and **F**) independent experiments. $n = 4$ replicates/group (**A**–**E**); $n = 6$ replicates/group (**F**). $^{**}P < 0.01$, $^{***}P < 0.001$, and $^{****}P < 0.0001$, by unpaired Student's $t$ test. Error bars indicate the SEM.

tor of Treg metabolic and functional fitness. PKC-θ co-binds with vimentin at the Treg DPC, and, based on phosphoproteomic data, vimentin is a phospho-target of PKC-θ. When vimentin integrity is disrupted by PKC-θ inhibition or direct vimentin knockdown, Treg-suppressive and metabolic function is enhanced and PKC-θ activity is reduced. Unexpectedly, the vimentin network was maintained, even in the absence of PKC-θ, and vimentin knockdown in germline PKC-θ-KO Tregs augmented their otherwise normal functional capacity, suggesting that the ability of vimentin to modulate Treg function is maintained, even in the absence of PKC-θ. A combination of vimentin knockdown and PKC-θ inhibition did not enhance Treg suppression above the level of vimentin knockdown alone, further indicating a key role for vimentin as an upstream modulator of Treg potency. Our findings reveal what we believe to be a novel role for vimentin in regulating Treg function by physically and functionally supporting processes that restrain Treg activity and point to vimentin targeting as a useful approach to enhancing in vivo Treg therapeutic efficacy.

This critical role for vimentin in regulating Treg suppression is, we believe, a particularly novel paradigm in T cell biology. While vimentin is known to be critical for maintaining structural integrity in circulating lymphocytes (36), this is the first time, to our knowledge, that a cytoskeletal protein other than actin or microtubules has been implicated as being important for controlling T cell function. Yet, unlike actin, which is a key positive mediator of T cell receptor (TCR) and CD28 signaling (37), vimentin participates in negative regulatory processes, making it only one of a few molecules known to act in such a capacity and the only molecule for which disruption prior to adoptive transfer augments Treg-mediated restraint of Tcon function in

vivo. Thus, we have revealed not only that vimentin is involved in modulating Treg activity but that, more broadly, cytoskeletal protein(s) can participate in the negative regulation of T cell functions. This paradigm is further supported by our preliminary data with the actin-uncapping protein RLTPR (also known as CARMIL2), which was identified in our phosphoproteomic screen. Knockdown of the RLTPR enhanced Treg function in in vitro suppression assays in a manner similar to that seen with vimentin siRNA (data not shown), suggesting a role for this molecule in Treg suppression. Since RLTPR interacts with both PKC-θ and vimentin (38, 39), we hypothesize that RLTPR facilitates linking between these critical proteins and that RLTPR knockdown results in a disruption of the vimentin network similar to that seen with vimentin knockdown and PKC-θ inhibition. Taken together, our extensive data on vimentin and preliminary data on RLTPR indicate that cytoskeletal proteins play a critical role in the negative regulation of T cell function.

Since disruption of the vimentin network augmented Treg metabolism, which is intimately linked with Treg function (33), we propose that at least one of the critical roles for vimentin in Tregs is to help control metabolic activity. We believe this is also novel, since no relationship between vimentin, or other intermediate filaments, and metabolic activity has ever, to our knowledge, been demonstrated in lymphocytes. In contrast to lymphocytes, vimentin is known to be intimately involved as a positive regulator of metabolic function in nonhematopoietic cells. In fibroblasts, vimentin acts as a scaffold for metabolic enzymes, while also promoting mitochondrial activity by altering mitochondrial migration and enhancing membrane potential, steps that are critical for maintaining respiratory chain physiology and generating ATP (40–42). Disrupting the interactions between vimentin and the mitochondria diminishes their metabolic activity, suggesting that appropriate contact between vimentin, metabolic enzymes, and the mitochondria is critical. In activated T cells, mitochondria are recruited to the IS (43, 44), where they participate in a variety of functions including calcium buffering (45), and in Tcons, vimentin also clusters to the IS after activation (46). In Tregs, the overall higher vimentin expression, paired with the densely packed vimentin network at the DPC, may result in altered mitochondrial recruitment to the cell membrane after activation, and vimentin disruption may then increase mitochondrial motility and function. Such mitochondrial effects may account for the increased Treg oxidative phosphorylation we observed. Support for this hypothesis includes the observations that vimentin residues 41–94 bind to mitochondria, and in cells in which vimentin organization is disrupted, mitochondrial motility is significantly enhanced (41). However, we also noted additional metabolic alterations, such as increased FA uptake and enhanced CTP1a expression, which would not be explained solely by this mitochondrial hypothesis. Since AEB071 caused detectable changes in 68 phospho-protein sites in activate Tregs (Supplemental Table 1), it is likely that other pathways are also involved, although, since both AEB071 and the highly specific PKC-θ inhibitor C20 had the same functional effect on Tregs (Supplemental Figure 2C and ref. 13), it is likely that the changes in downstream pathways we observed after AEB071 treatment were due to direct effects of the drug on PKC-θ, and not to off-target effects.

One such critical pathway downstream of PKC-θ and vimentin may be the mTORC2 signaling cascade. Our data demonstrate a role for vimentin and PKC-θ in mTORC2 regulation, which expands upon previous work showing that modulation of mTORC1/2 activity significantly alters Treg metabolic fitness and function (30, 31, 34). Disruption of vimentin was associated with diminished downstream mTORC2 signaling, including reduced AKT (Ser473) and Foxo3a phosphorylation, which may favor the balance toward mTORC1 signaling, even without overtly augmenting mTORC1 activity, thereby promoting increased FA uptake, oxidative phosphorylation, and CPT1a expression. This altered mTORC1/2 balance is similar to that seen in PTEN-KO mice, in which an overactivation of mTORC2 skews the mTORC1/2 activity ratio toward mTORC2, even without changing baseline mTORC1 function, and significantly changes Treg function and metabolism (31).

While no direct link between mTOR and vimentin has been made in T cells, there is a clear relationship between mTOR proteins and vimentin in cancer cells. Specifically, mTOR overactivation stimulates excessive vimentin expression in epithelial tumor cells, which drives metastatic transformation and disease progression (47). In contrast to observations in cancer, our data support a reciprocal regulatory process, in which vimentin network integrity is important for downstream mTORC2 signaling. This role for vimentin is similar to the one that it plays in NLRP3 and NOD/NLRP1 inflammasome signaling in immune cells, in which vimentin's scaffold function is a critical upstream component of these cascades (48, 49). Additionally, our data suggest that vimentin-mediated support of PKC-θ may in turn bolster mTORC2 function through the intermediary molecule IKK (27, 50). Together, these data suggest that the integrity of the vimentin network, and perhaps vimentin's role as a scaffold protein, may be important for mTORC2 activity and subsequent metabolic regulation in Tregs.

The relationship between vimentin and mTORC2 may also be critical for the augmentation in Treg suppression of antigen-specific priming we observed. mTORC2 drives phosphorylation-dependent nuclear exclusion of Foxo3a, a process that limits Treg function and expression of Lag3 and Nrp1 (19, 26) (DECODE database, http://gncpro.sabiosciences.com). In this context, our data demonstrating reduced phosphorylation of Foxo3a after vimentin modulation may explain the increased Nrp1 and Lag3 expression we observed, as reduced Foxo3a phosphorylation augmented nuclear translocation and transcriptional activation. Since Nrp1 and Lag3 are important for suppressing Tcon priming (51, 52), augmented expression of these molecules, in combination with metabolic alterations, probably contributed to the increased inhibition of alloantigen-specific Tcon priming we observed in vivo in mice with GVHD. This decrease in antigen-specific priming probably drove the reductions in Tcon metabolic activity, cytokine production, and GVHD progression we observed, as priming is critical for initiating Tcon metabolic changes and effector differentiation (33). Furthermore, Tregs exert much of their suppressive effect in GVHD early in the course of the disease. Tregs and Tcons home to secondary lymphoid organs within hours of infusion, and Tregs unable to home to secondary lymphoid organs cannot suppress GVHD

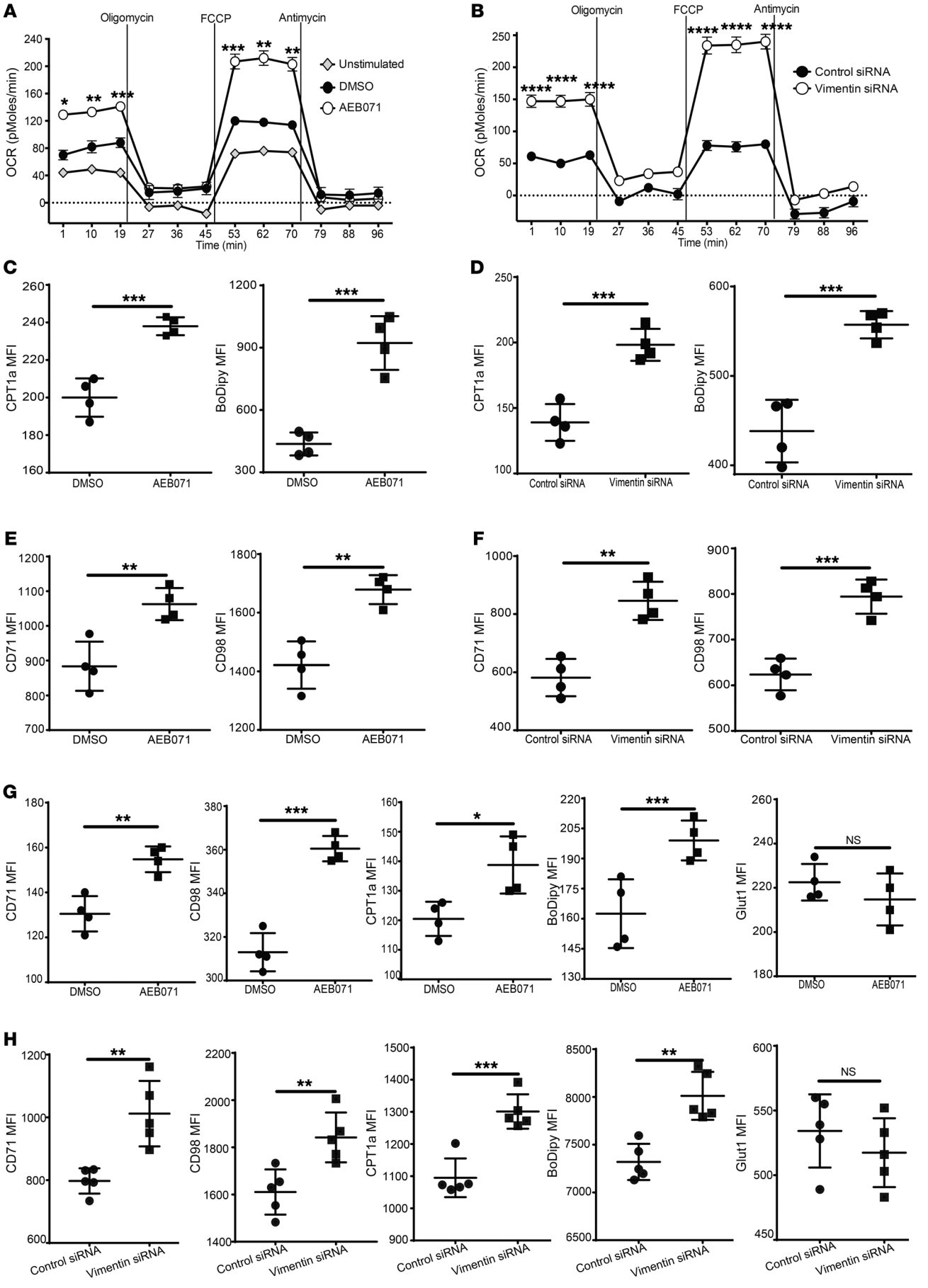
A
Oligomycin
FCCP
Antimycin
OCR (pMoles/min)
Time (min)
Unstimulated
DMSO
AEB071
B
Oligomycin
FCCP
Antimycin
OCR (pMoles/min)
Time (min)
Control siRNA
Vimentin siRNA
C
CPT1a MFI
BoDipy MFI
DMSO
AEB071
D
CPT1a MFI
BoDipy MFI
Control siRNA
Vimentin siRNA
E
CD71 MFI
CD98 MFI
DMSO
AEB071
F
CD71 MFI
CD98 MFI
Control siRNA
Vimentin siRNA
G
CD71 MFI
CD98 MFI
CPT1a MFI
BoDipy MFI
Glut1 MFI
NS
DMSO
AEB071
H
CD71 MFI
CD98 MFI
CPT1a MFI
BoDipy MFI
Glut1 MFI
NS
Control siRNA
Vimentin siRNA

**Figure 7. Vimentin disruption augments Treg metabolic activity.** (**A** and **B**) OCR analysis of activated Tregs either (**A**) pretreated with DMSO or AEB071 or (**B**) transfected with control or vimentin siRNA. (**C**–**F**) Analysis of splenic donor Tregs on day 4 after GVHD transplantation, with recipient mice given BM plus Tcons plus Tregs. (**C** and **D**) CPT1a expression and $BoDipy_{C1-C12}$ uptake on donor Tregs (**C**) pretreated with DMSO or AEB071 or (**D**) transfected with control or vimentin siRNA. (**E** and **F**) Expression of receptors for iron (CD71) and amino acids (CD98) on donor Tregs (**E**) pretreated with DMSO or AEB071 or (**F**) transfected with control or vimentin siRNA. (**G** and **H**) Analysis of CD71, CD98, CPT1a, and Glut1 expression as well as $BoDipy_{C1-C12}$ uptake in Tregs isolated from recipient mouse small intestine LP on day 14 after transplantation. Tregs were either (**G**) pretreated with DMSO or AEB071 or (**H**) transfected with control or vimentin siRNA. Data are from 1 representative experiment of 3 independent experiments. $n$ = 5 replicates/group (**A** and **B**); $n$ = 5 mice/group (**H**); and $n$ = 4 mice/group (**C**–**G**). $^{*}P < 0.05$, $^{**}P < 0.01$, $^{***}P < 0.001$, and $^{****}P < 0.0001$, by unpaired Student's $t$ test. Error bars indicate the SEM.

(53, 54). Therefore, we posit that augmented inhibition of early events critical to GVHD pathogenesis, such as alloreactive Tcon priming, by AEB071- and vimentin siRNA–treated Tregs suppresses GVHD development and progression and accounts for the reduction in GVHD-related mortality and severity.

Given our results, we further propose that the previously unknown mechanism behind mTORC2-KO rescue of PTEN-deficient Treg function (30) may be an augmented expression of Nrp1 and Lag3 and metabolic activity. Together, our data suggest that vimentin plays key roles in a multitude of Treg functional and metabolic processes and demonstrate novel relationships between vimentin and a variety of signaling pathways, none of which, to our knowledge, have been described previously in lymphocytes.

Finally, our findings support a model in which vimentin interacts with PKC-θ, and probably a variety of other downstream kinases, to promote signaling that restrains Treg fitness (Supplemental Figure 8, A and B). On the basis of this model, we posit that vimentin is a crucial upstream molecule involved in limiting Treg activity during immune responses. While Tregs require TCR/CD28 signaling for their function (55, 56), mTORC2/AKT signaling induces TCR/CD28 signaling, which is in turn dampened by PD-1 and CLTA-4, two molecules critical for optimal Treg potency (57, 58). Since disruption of vimentin augmented Treg suppression and reduced mTORC2 signaling, this suggests that the vimentin network, and the pathways it supports, may oppose signaling that promotes Treg function, such as the PD-1 and CTLA-4 pathways, via mTORC2 effects. This type of parallel, but oppositional, regulation mimics Tcon costimulation/coinhibition and may be important for tuning Treg activity within different immunological contexts. Overall, our data suggest that the vimentin network acts as a regulator of Treg functional and metabolic fitness and demonstrate that targeting this structure is a novel method for improving the in vivo therapeutic efficacy of adoptively transferred Tregs, as demonstrated in a model of GVHD lethality.

## Methods

*Mice*. C57BL/6 (B6, $H2^{b}$), B6 CD45.1, B6 Thy1.1, and BALB/c ($H2^{d}$) mice were purchased from Charles River Laboratories. CB6.F1-CD11c-YFP ($H2^{b}/H2^{d}$), B6 luciferase–transgenic, and B6 Foxp3-GFP mice were bred under in-house veterinary staff guidance. B6 OVA TCR–transgenic OT-I mice and B6 ubiquitin eGFP TCR–transgenic TEα mice were provided by Brian Fife (University of Minnesota, Minneapolis, Minnesota, USA). Mice were housed in a specific pathogen–free facility and used with the approval of the IACUC of the University of Minnesota.

*GVHD models and T cell purification*. A C57BL/6→BALB/c acute GVHD (aGVHD) model was used as described previously (22). Briefly, BALB/c mice were irradiated with 7.0 Gy total body irradiation (TBI) on day –1 and then i.v. injected on day 0 with $10^7$ B6 BM ± $2 \times 10^6$ B6 Tcons alone or Tcons plus $1 \times 10^6$ B6 Tregs. Splenic Tcons were purified by negative selection using biotin anti-CD19 (1D3), CD11b (M1/70), CD11c (N418), NK1.1 (PK136), CD49b (DX5), CD25 (PC61.5), and TER-119 Abs (all from STEMCELL Technologies), followed by streptavidin RapidSpheres depletion with an EasySep Magnet (STEMCELL Technologies). Lymph node and splenic Tregs were purified using negative selection as above, but with the addition of anti-CD8 Ab (53–6.7, STEMCELL Technologies) and removal of anti-CD25 to enrich $CD4^+$ T cells. $CD4^+$ T cells were incubated with phycoerythrin-labeled (PE-labeled) anti-CD25 (PC61.5, eBioscience), followed by anti-PE beads (Miltenyi Biotec). $CD25^+$ cells were selected with magnetic columns (Miltenyi Biotec). For 2-photon imaging experiments, CB6.F1-CD11c-YFP recipient mice were irradiated with 11.0 Gy TBI on day –1 and then injected i.v. on day 0 with $10^7$ B6 BM and $5 \times 10^6$ B6 polyclonal Tregs. On day two, $10 \times 10^6$ OT-I $CD8^+$ T cells and $1 \times 10^6$ eGFP TEα $CD4^+$ T cells were given. OT-I T cells were labeled with CellTrace Violet (Life Technologies, Thermo Fisher Scientific) or Cell Tracker Orange (Life Technologies, Thermo Fisher Scientific) following the manufacturer's the protocol.

*In vivo BLI*. In vivo BLI was performed as described previously (59). Briefly, firefly luciferin substrate (0.1 ml at 30 mg/ml, Promega) was i.p. injected into recipient mice 5 minutes before imaging. A Xenogen in vivo imaging system (IVIS) was used to quantify luminescence. Luminescence was captured for 1 minute, and data were analyzed with Living Image 3.0 software (Calipers).

*Multiphoton microscopy*. Mesenteric and brachial lymph nodes were removed from recipient mice 3 hours after i.p. injection of 200 μg anti-CD62L mAb (MEL-14, eBioscience), immobilized on coverslips, and perfused with 37°C RPMI with 95% $O_2$ and 5% $CO_2$. Samples were excited with a MaiTai TiSaphire DeepSee HP Laser (12W, Spectra-Physics) at 870 nm, and emissions of 440 to 480 nm (CellTrace Violet), 500 to 520 nm (GFP), 520 to 560 nm (YFP), and 560 to 630 nm (CMTMR) were collected. A 4-channel Leica TCS MP microscope with a resonant scanner containing 2 NDD and 2 HyD photomultiplier tubes operating at the video rate was used to capture images. Images acquired were 50–250 μm below the capsule. *XY* frames (512 × 512) were collected at 3.0-μm steps every 30 seconds for 30 minutes. Image stacks were unmixed with LAS AF 3.0 software (Lecia Microsystems). 3D images, time-lapse movies, and cell tracks were generated with Imaris 8.2 × 64 software (Bitplane). Tracks were verified manually, and tracking data were analyzed with a custom macro in Microsoft Excel, as described previously (60). The confinement ratio was the distance from the origin/track displacement.

*Intestinal lymphocyte isolation*. Lamina propria (LP) lymphocytes were isolated using a previously described protocol (22) with modifications. In brief, after removing and flushing small intestines, tissues were cut longitudinally and then into 2- to 3-cm pieces and washed twice in Ca/Mg-free PBS with 5 mM EDTA (G-Biosciences) and 10

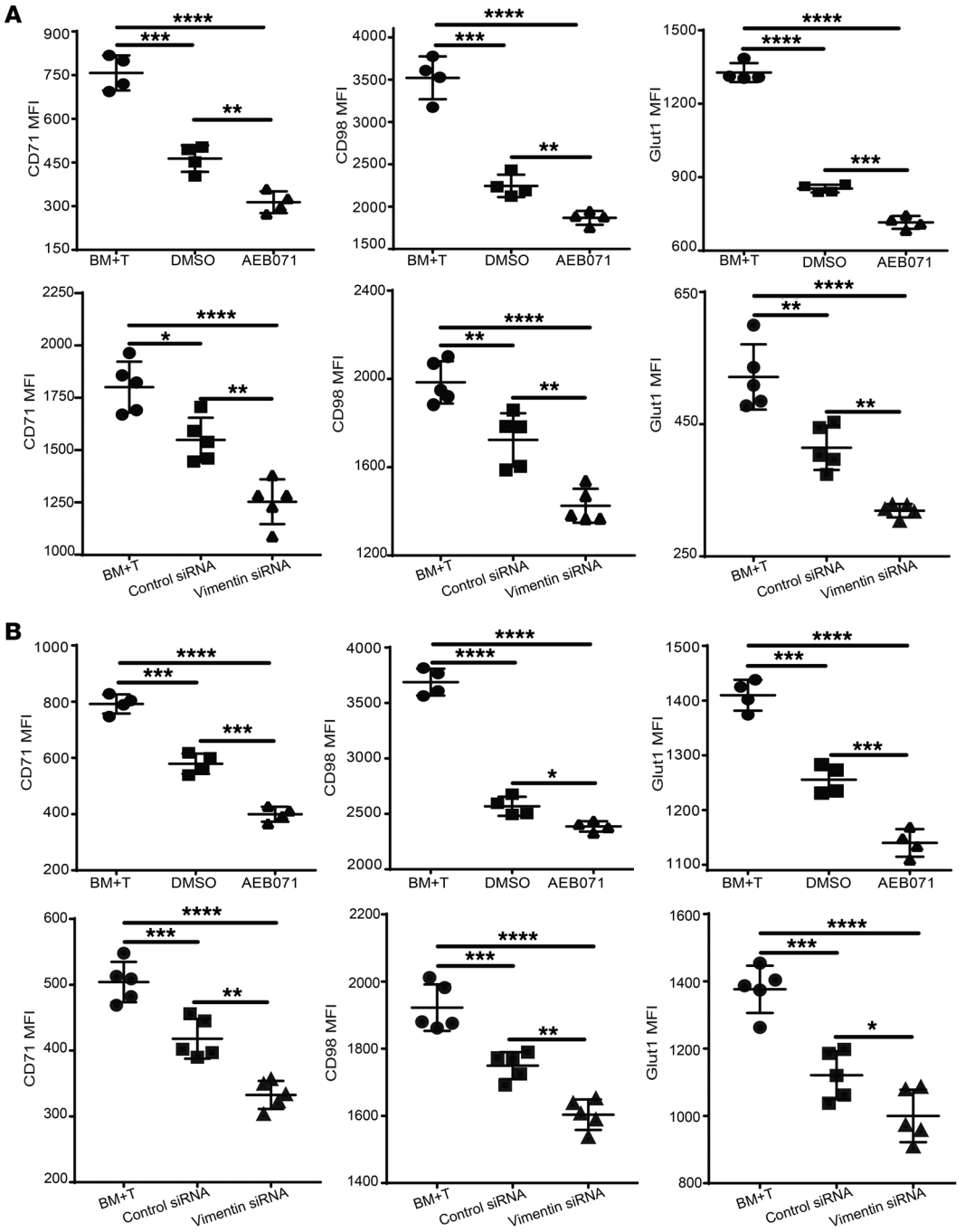


**Figure 8. Vimentin disruption augments Treg-mediated suppression of Tcon metabolic activity in the spleen.** (**A** and **B**) GVHD transplantation, with recipient mice given either BM plus Tcons or BM plus Tcons plus Tregs. Tregs were pretreated with DMSO or AEB071 or transfected with control or vimentin siRNA. Analysis of CD71, CD98, and Glut1 expression on donor splenic (**A**) $CD4^+$ and (**B**) $CD8^+$ Tcons on day 4 after transplantation. Data are from 1 representative experiment of 3 independent experiments. $n$ = 5 mice/group for control and vimentin siRNA transplants; $n$ = 4 mice/group for DMSO and AEB071 transplants. $^*P < 0.05$, $^{**}P < 0.01$, $^{***}P < 0.001$, and $^{****}P < 0.0001$, by unpaired 1-way ANOVA with multiple comparisons analysis and Tukey's post test. Error bars indicate the SEM.

mM HEPES (Sigma-Aldrich) (10 min, 37°C). Tissues were then cut into smaller pieces and treated 3 times with 1 mg/ml collagenase D (Roche), 0.15 IU/ml dispase (Sigma-Aldrich), and 0.5 mg/ml DNAseI (Roche) in Ca/Mg-free PBS with 10% FBS (20 min at 37°C). Lymphocytes were purified on a 40%/80% Percoll gradient (2,500 rpm, 20°C, 20 min). Percoll was diluted in fully supplemented RPMI media.

*Histopathology*. Colons, small intestines, livers, and spleens were harvested on day 14 after transplantation, embedded in OCT compound (Miles), snap-frozen, and stored at –80°C. Frozen blocks were cut into 5-μm sections and mounted onto microscope slides (Superfrost/Plus, Thermo Fisher Scientific). Sections were fixed and stained with H&E (Thermo Fisher Scientific) according to the manufacturer's

instructions. Stained slides were examined in a blinded fashion using a semiquantitative scoring system as previously described (22).

*Immunofluorescence*. Freshly purified mouse Tregs were activated for 10 minutes on anti-CD3–coated (10 μg/ml, 145-2C11, eBioscience), anti-CD28–coated (2.5 μg/ml, 37.51, eBioscience), and ICAM-coated (5 μg/ml) sticky-Slides VI 0.4 (Ibidi). Cells were pretreated with inhibitors (see below) and/or anti-CD25 mAb–coated nanoparticles (15 min, room temperature; Miltenyi Biotec) prior to activation. Cells were fixed for 10 minutes in 2% PFA in PHEM buffer (60 mM PIPES, 25 mM HEPES, 10 mM EGTA, 2 mM $MgCl_2$, pH 6.9) and permeabilized for 3 minutes with 0.01% Triton X-100. Cells were blocked with 5% casein for 1 hour, incubated with a primary mAb for 1 hour, followed by incubation with a fluorescent secondary mAb for 30 minutes. Between staining, cells were washed with 1 ml HBSS-HSA. ProLong Gold Antifade Mountant with DAPI (Life Technologies, Thermo Fisher Scientific) was added to the slide chambers after staining. Tregs were stained with Cy3 anti-vimentin (D21H3, Cell Signaling Technology), purified PKC-θ (C-18, Santa Cruz Biotechnology), or biotin anti-Foxp3 (FJK-16s, eBioscience) mAb. Secondary staining was done with AF488 or AF647 donkey anti–goat or anti–rabbit Fab2 fragments (Jackson ImmunoResearch). Biotin primary mAbs were stained with Cy5-streptavidin (Jackson ImmunoResearch). Imaging was performed on a laser scanning confocal Zeiss LSM-710 with 488-, 543-, and 633-nm lasers, a ×63 objective with 1.4 NA, and the pinhole set to 1 Airy unit. *Z*-stacks were taken at 340-nm intervals.

*PKC-θ and IKK inhibitor treatment*. The PKC-θ inhibitor AEB071 (Selleckchem) and IKK inhibitor BAY 11-7082 (Calbiochem) were reconstituted in DMSO and stored according to the manufacturer's instructions. Tregs were incubated with 10 μM AEB071, 10 μM BAY 11-7082, or an equivalent volume of DMSO for 30 minutes at 37°C. After incubation, Tregs were washed in warmed, fully supplemented RPMI media to remove excess inhibitor or DMSO.

*siRNA treatment*. Freshly purified mouse Tregs were transfected by electroporation as described previously (13) with 5 μM mouse vimentin, PKC-θ, or nontargeting control siRNA (GE Dharmacon). Electroporation was performed using the Mouse T cell Nucleofector Kit (Lonza) and a Nucleofector 2b machine (Amaxa) on setting X-001.

*Mouse T cell stimulation*. For suppressive molecule analysis, freshly purified mouse Tregs were stimulated for 48 hours at 37°C with in-house–generated anti-CD3 mAb– and anti-CD28 mAb–coated beads with 1,000 IU/ml recombinant human IL-2 (rhIL-2, Novartis). For metabolic and Seahorse metabolic assays, freshly purified mouse Tregs were stimulated for 18 hours at 37°C with anti-CD3 mAb– and anti-CD28 mAb–coated beads with 1,000 IU/ml rH IL-2. For phosphoflow analysis, freshly purified mouse Tregs were stimulated for 5 or 60 minutes at 37°C with plate-bound 10 μg/ml anti-CD3 and anti-CD28 mAbs. For cytokine analysis, cells were incubated for 5 hours at 37°C with 1× eBioscience Cell Stimulation Cocktail. Stimulation beads were made by conjugating equimolar quantities of anti-CD3 (145-2C11, eBioscience) and anti-CD28 (37.51, eBioscience) mAbs to M-450 Tosylactivated Dynabeads (Life Technologies, Thermo Fisher Scientific), using an optimized version of the manufacturer's protocol.

*Suppression assays and CFSE staining*. Freshly purified mouse Tcons were labeled with 2.5 μM CFSE (Life Technologies, Thermo Fisher Scientific) for 10 minutes at 37°C. Tcons were mixed with DMSO- or AEB071-treated mouse Tregs at Treg/Tcon ratios of 0:1, 1:1, 1:3, and 1:9 in the presence of soluble anti-CD3 mAb (0.25 μg/ml, 145-2C11, eBioscience) and T cell–depleted mouse splenocytes. The ratios were plated in quadruplicate. CFSE dilution was analyzed after 72 hours by flow cytometry. In certain experiments, blocking mAbs against Nrp1, Lag3, or both were added to some cultures. Anti-Nrp1 (761704, R&D Systems) was used at 25 μg/ml, and anti-Lag3 (C9B7W, eBioscience) was used at 60 μg/ml.

Transwell assays were performed as described previously (19). Briefly, B6 Foxp3-GFP mouse Tregs were flow sorted and treated with DMSO or AEB071. $CD4^+$ mouse Tcons were isolated as above and CFSE labeled. Additional mouse Tcons (no CFSE) were fixed for 5 minutes at room temperature in 4% PFA. Tcons were mixed with anti-CD3 mAb– and anti-CD28 mAb–coated beads (Dynabeads, Thermo Fisher Scientific) at a 1:1 bead/cell ratio. Tcons (50,000 cells) were plated in the bottom of a Transwell (EMD Millipore). Mesh inserts (0.4-μM pore size) were placed. Tregs were mixed with anti-CD3– and anti-CD28–coated beads at a 2:1 bead/cell ratio. Tregs (15,000 cells) and fixed $CD4^+$ Tcons (45,000 cells) were placed on top of the inserts. Conditions were plated in quadruplicate. CFSE dilution was analyzed after 72 hours. A blocking mAb against Nrp1 or Lag3 was added as described above.

For in vivo experiments, freshly purified $CD4^+$ and $CD8^+$ mouse Tcons were labeled with CFSE for 20 minutes at 37°C prior to infusion. Some mice also received DMSO- or AEB071-treated mouse Tregs. Spleens were harvested 72 hours after cell infusions and analyzed by flow cytometry for Tcon CFSE dilution.

*Metabolic flux analysis*. The oxygen consumption rate (OCR) and extracellular acidification rate were measured using the XF-24 Extracellular Flux Analyzer (Seahorse Bioscience) in XF media (DMEM with 25 mM glucose, 1× GlutaMAX, and 1 mM sodium pyruvate). The OCR was measured under basal conditions and in response to 1 μM oligomycin, 1 μM fluorocarbonyl cyanide phenylhydrazone, and 1 μM antimycin. The extracellular acidification rate (ECAR) was measured under basal conditions and in response to 20 mM glucose, 1 μM oligomycin, and 80 mM 2-deoxyglucose.

*Flow cytometry*. Single-cell suspensions were recorded on a BD LSRFortessa flow cytometer. FCS3.0 files were analyzed using FlowJo, version 10. The following Abs were purchased from eBioscience or BioLegend: anti-CD4 (RM4-5/GK1.5), anti-CD8 (53-6.7), anti-CD25 (PC61.5), anti-CD45.1 (A20), anti-CD71 (R17217), anti-CD73 (TY/11.8), anti-CD98 (RL388), anti-Thy1.1 (HIS51), anti–CTLA-4 (UC10-4B9), anti-ICOS (7E.17G9), anti-Nrp1 (3DS304M), anti-Lag3 (C9B7W), anti-Foxp3 (FJK-16s), anti–IFN-γ (XMG1.2), and anti–TNF-α (MP6-XT22). Anti–PKC-θ (C-18) was obtained from Santa Cruz Biotechnology. Anti-vimentin (D21H3), phosphorylated AKT (p-AKT) (Ser473) (D9E), p-AKT (Thr308) (C31E5E), p-S6 (Ser235/236) (D57.2.2E), and p–4E-BP1 (Thr37/46) (236B4) were obtained from Cell Signaling Technology. Polyclonal anti–p–PKC-θ (Ser676) and anto-Foxo3a (Ser253) were purchased from Santa Cruz Biotechnology and Abcam, respectively. Anti-CPT1A (8F6AE9) and anti-Glut1 (EPR3915) Abs were obtained from Abcam. Cells were stained with Fixable Viability Dye ef780 or ef450 (eBioscience) for all experiments. For some experiments, cells were surface stained and then stained with tetramethylrhodamine-methyl ester-perchlorate (TMRM), MitoTracker Deep Red, or $BoDipy_{C1–C12}$ 500/510 (all from Life Technologies, Thermo Fisher Scientific), following the manufacturer's protocols. Fixation and intracellular and intranuclear

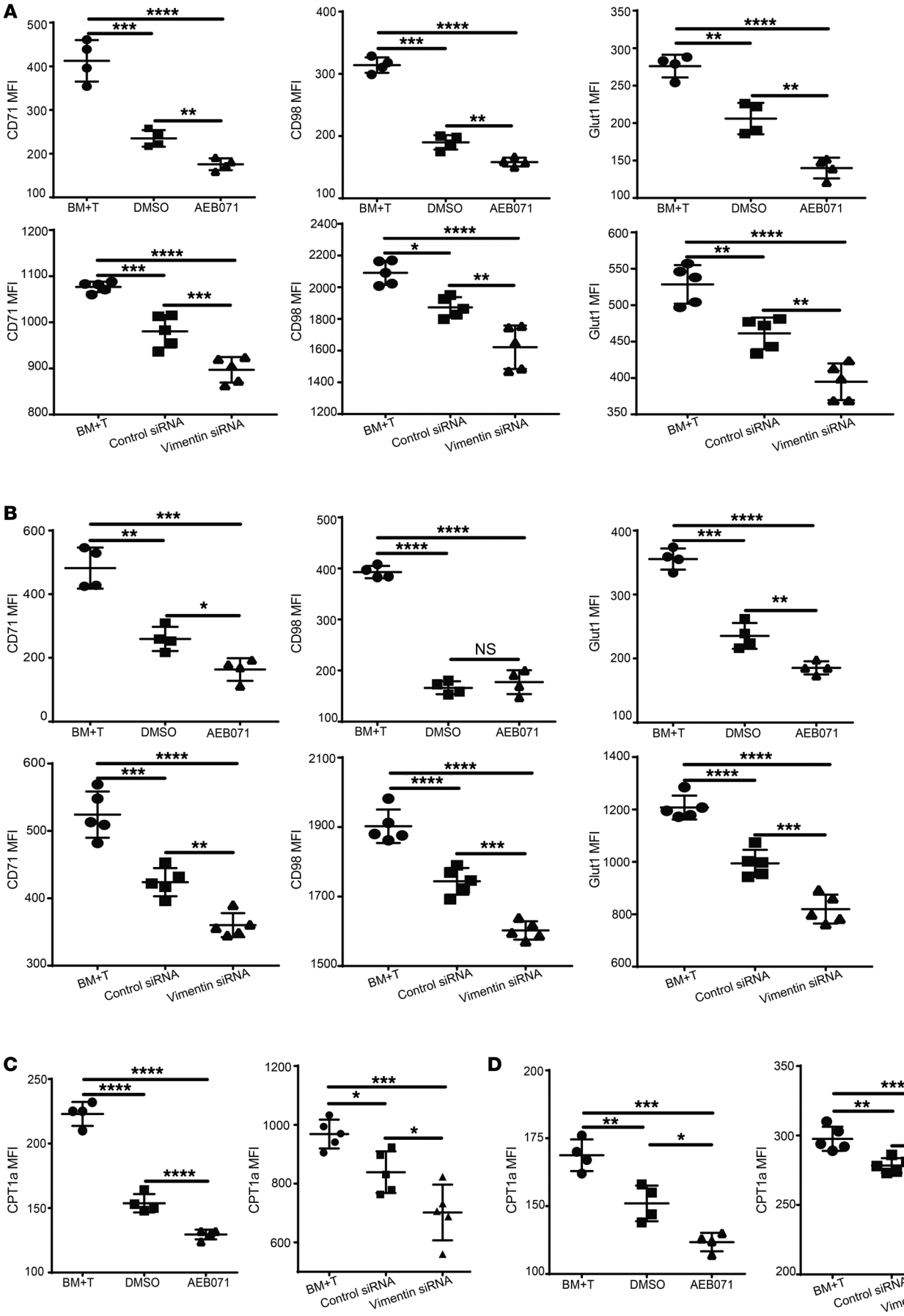
A
CD71 MFI
CD98 MFI
Glut1 MFI
BM+T
DMSO
AEB071
Control siRNA
Vimentin siRNA
B
NS
C
CPT1a MFI
D

**Figure 9. Vimentin disruption with siRNA augments Treg-mediated suppression of Tcon metabolic activity in the small intestine.** (**A**–**F**) GVHD transplant with recipient mice given either BM plus Tcons or BM plus Tcons plus Tregs. Tregs were pretreated with DMSO or AEB071 or transfected with control or vimentin siRNA. Tcons were isolated from recipient mouse small intestine LP on day 14 after transplantation. (**A** and **B**) Expression of CD71, CD98, and Glut1 on donor (**A**) $CD4^+$ and (**B**) $CD8^+$ Tcons. (**C** and **D**) Expression of CPT1a on (**C**) $CD4^+$ and (**D**) $CD8^+$ Tcons. Data are from 1 representative experiment of 3 independent experiments. $n = 4$ mice/group for DMSO and AEB071 transplants; $n = 5$ mice/group for control and vimentin siRNA transplants. $^*P < 0.05$, $^{**}P < 0.01$, $^{***}P < 0.001$, and $^{****}P < 0.0001$, by 1-way ANOVA with multiple comparisons analysis and Tukey's post test. Error bars indicate the SEM.

staining were done using either the eBioscience Foxp3 Staining Kit or the eBioscience IC Fixation Kit. For phosphoflow analysis, cells were stained using a modified version of the eBioscience Protocol B, including incubation with Fixable Viability Dye prior to fixation. The compatibility of phosphorylation-specific Abs with fixation and permeabilization buffers was verified by the manufacturer and then tested in-house to ensure efficacy.

*Human Treg culture and SILAC labeling for phosphoproteomic screening*. Naive human Tregs were flow sorted from peripheral blood apheresis products, stimulated with anti-CD3–loaded (OKT3, BD Biosciences) artificial APCs, and then expanded in heavy or light SILAC media (see below) with 300 IU/ml recombinant human IL-2 (Novartis). On day 14, Tregs were restimulated with anti-CD3 mAb– and anti-CD28 mAb–coated beads (Dynabeads Human T-Expander, Thermo Fisher Scientific). On day 21 of culture, cells were isolated from culture and beads were removed.

After bead removal, Tregs were incubated with DMSO or AEB071, washed with cold media, incubated with soluble anti-CD3 (1 μg/ml, OKT3, BD Biosciences) and anti-CD28 (1 μg/ml, 28.2, BD Biosciences) mAbs on ice for 30 minutes and then washed in cold media. Tregs were then acutely stimulated for 10 minutes using anti–mouse IgG Fab2 (1 μg/ml, Jackson ImmunoResearch) to cross-link the anti-CD3 and anti-CD28 mAbs. Cells were then washed, spun down, and the pellets snap-frozen.

Heavy/light SILAC media contained SILAC RPMI-1640 (Invitrogen, Thermo Fisher Scientific) supplemented with FBS (Invitrogen, Thermo Fisher Scientific), 10 mM L-glutamine, 1× nonessential amino acids, 0.5× penicillin/streptomycin, and 0.05 mM 2-ME (Gibco, Thermo Fisher Scientific). Heavy media were supplemented with Lys8 and Arg12 (Cambridge Isotopes) and light media with unlabeled Lys/Arg.

*Phosphopeptide enrichment for liquid chromatography–mass spectrometry*. Human Treg pellets (from above) were lysed in urea buffer (8 M Urea, 50 mM Tris, pH 7.5, 150 mM NaCl, 1 mM EDTA, 2× protease inhibitor Roche), 2× PhosSTOP (Roche), and 1 mM chloroacetamide (Roche), solubilized for 10 minutes, sonicated using a Bioruptor (Diagenode) for 3 minutes with a 50% duty cycle, and clarified by centrifugation (14,000 rpm for 10 min). Extract was reduced with 5 mM DTT for 45 minutes, acetylated with 10 mM chloroacetamide for 30 minutes, and quenched with 5 mM DTT for 20 minutes (20°C, dark). Samples were diluted to 2 M urea using 50 mM Tris, pH 7.5, 150 mM NaCl, and 2 mM $CaCl_2$ and digested with Trypsin Gold (Promega) at a 1:50 trypsin/protein ratio for 16 hours at 37°C. The peptides were acidified by addition of trifluoroacetic acid (TFA) to 0.4%, clarified as above, and then desalted on a 10-mg Sep-Pak C18 column (Waters) and speed-vacuumed. Peptides were fractionated using hydrophilic interaction liquid chromatography (HILIC) on an Agilent 1100 HPLC using a TSKgel Amide-80 column (W00202-89T, Tosoh). An 80% acetonitrile (ACN) gradient with 0.1% TFA was decreased to 0% ACN with 0.1% TFA over 60 minutes at a 0.3-ml/minute flow rate, with fractions collected every 4 minutes, followed by drying in a speed vacuum. Each fraction was reconstituted in 3% TFA and 60% ACN and processed through TiO2 Beads (GL Science) packed in-house into a 10-μl stage tip with a C8 plug. Enrichment was performed as described previously (61), and eluted phosphopeptides were speed-vacuumed to dryness and then reconstituted in 6 μl 4%FAs and 2% ACN prior to liquid chromatography–mass spectrometry (LC-MS). All steps were performed at 4°C unless otherwise noted.

*LC-MS and data analysis*. An EASY-nLC1000 coupled to a QExactive Mass Spectrometer (both from Thermo Fisher Scientific) were used as described previously (17). Briefly, a self-packed 75 μm × 25 cm reversed-phase column (Reprosil C18, 3 μm, Dr. Maisch GmbH) was used for separation. Peptides were eluted by a gradient of 3% to 30% ACN in 0.1%FAs over a 180-minute period at a rate of 250 nl/min (45°C). The QExactive was operated in data-dependent mode, with survey scans acquired at a resolution of 50,000 at $m/z$ 400 (transient time = 256 ms). Up to 10 of the most abundant precursors with an isolation window of 1.6 thomsons were selected from the survey scan and fragmented by higher-energy collisional dissociation with normalized collision energies of 27. The maximum ion injection times for the survey scan and the MS/MS scans were 60 ms, respectively, and the ion target value for both scan modes was set to 1 million.

*Electron microscopy*. Freshly purified mouse Tregs were activated on anti-CD3–, anti-CD28–, and ICAM-coated coverslips (as above). Cells were then fixed in a solution of 1% glutaraldehyde, 3% paraformaldehyde (PFA), and 0.3% tannic acid in 0.1 M cacodylate buffer, pH 7.4, for 1 hour at room temperature and processed for electron microscopic analysis (62). Coverslips were removed and cells postfixed with 1% osmium tetroxide in 0.1 M cacodylate buffer, pH 7.4, for 1 hour at room temperature. Samples were then dehydrated in a solution series containing 25%–100% ethanol and flat-embedded by placing upturned BEEM capsules containing liquid epoxy resin (Epon) over the coverslips. Capsules were stabilized with weights to ensure firm contact with the coverslips and cured at 60°C for 48 hours. Capsules were detached from the coverslips by immersion in liquid nitrogen, and polymerized resin blocks containing embedded Tregs and anti-CD3/anti-CD28/ICAM layers were isolated. Blocks were re-embedded in Epon to obtain cross-sectional views of the Treg-mAb interface, with sections cut using a Leica UCT ultramicrotome, orthogonal to the plane of the embedded interface. At least 3 serial sections were used to determine the plane nearest to the cell center.

*Statistics*. Data are reported as mean values ± SEM. Pairs were compared using unpaired, 2-tailed Student's $t$ tests. Data sets with 3 or more samples were compared using 1-way ANOVA with multiple comparisons analysis, including a Tukey's post hoc test with correction for multiple comparisons. Differences in survival were analyzed by log-rank test. A $P$ value of less than 0.05 was considered statistically significant. All non–LC-MS statistical analyses were performed using GraphPad Prism 6 (GraphPad Software). LC-MS data were analyzed as described previously (17). In brief, raw files were processed using the MaxQuant computational proteomics platform (version 1.2.7.0), and analysis using Perseus software (version 1.4.1.3) included a significance B test with Benjamini-Hochberg correction and a 0.05% FDR.

*Study approval*. Animals studies were conducted in accordance with a protocol reviewed and approved by the IACUC of the University of Minnesota (1804-35814A). The human cells utilized in this study were derived from leukapheresis products purchased from the Memorial Blood Center (St. Paul, Minnesota, USA). No approval was required for these purchased human samples.

## Author contributions

CMH designed and performed experiments, discussed results, and wrote the manuscript. JTM designed and performed experiments, discussed results, and edited the manuscript. GT, ML, AS, SK, DKR, MJS, GZ, BHK, JL, JSM, CF, AKK), and BTF performed experiments, discussed results, and edited the manuscript. APM performed histologic analyses and edited the manuscript. MJO contributed to experimental design and edited the manuscript. KLH and AK contributed to experimental design, discussed results, and edited the manuscript. JSS, HC, and DHM discussed results and edited the manuscript. TAN, LAT, MLD, and BRB contributed to experimental design, discussed results, and edited the manuscript.

## Acknowledgments

The authors thank Amnon Altman (La Jolla Institute for Allergy and Immunology) for his commentary, David Bernlohr and Rocio Foncea (Department of Biochemistry, Molecular Biology and Biophysics, University of Minnesota), and the Minnesota Obesity Center for assistance with the Seahorse experiments. This work was funded by the National Institute of Allergy and Infectious Diseases (NIAID), the National Heart, Lung, and Blood Institute (NHLBI), the National Cancer Institute (NCI), the National Center for Research Resources (NCRR), the National Center for Advancing Translational Sciences (NCATS), and the National Institute of Diabetes and Digestive and Kidney Diseases (NIDDK) of the NIH under grant numbers P01 AI056299, R01 HL56067, AI112613, AI34495, and P01 CA142106 (to BRB); R01 AI043542 (to MLD); T32 AI007313 and F30 HL121873 (to CMH); R01 AI106791 (to BTF); R01 CA157971 (to AK); R01 AI191497 and R01 AI105887 (to HC); S10 RR027990 (to TAN); S10 RR023704-01A1 (NYUSOM Microscopy Core); P30 DK050456 (MN Obesity center); and P01 AI056299 (to LAT). The Zeiss 710 MP microscope was purchased in part with funds from NIH grant RR023704-01A1. The Nikon TIRFM was purchased with funds from NIH grants P01AI080192 and R37AI043542. We thank M. Cammer for support with light microscopy and F. Liang for electron microscopy assistance through the NYULMC Office of Collaborative Science Microscopy Core.

Address correspondence to: Bruce R. Blazar, MMC 109, University of Minnesota, 420 Delaware St SE, Minneapolis, Minnesota 55455, USA. Phone: 612.626.2734; Email: blaza001@umn.edu.

1. Ohkura N, Kitagawa Y, Sakaguchi S. Development and maintenance of regulatory T cells. *Immunity*. 2013;38(3):414–423.
2. Sakaguchi S, Yamaguchi T, Nomura T, Ono M. Regulatory T cells and immune tolerance. *Cell*. 2008;133(5):775–787.
3. Tanaka A, Sakaguchi S. Regulatory T cells in cancer immunotherapy. *Cell Res*. 2017;27(1):109–118.
4. Newton R, Priyadharshini B, Turka LA. Immunometabolism of regulatory T cells. *Nat Immunol*. 2016;17(6):618–625.
5. McDonald-Hyman C, Turka LA, Blazar BR. Advances and challenges in immunotherapy for solid organ and hematopoietic stem cell transplantation. *Sci Transl Med*. 2015;7(280):280rv2.
6. Blazar BR, Murphy WJ, Abedi M. Advances in graft-versus-host disease biology and therapy. *Nat Rev Immunol*. 2012;12(6):443–458.
7. Pasquini M, Wang Z. Current Uses and Outcomes of Hematopoietic Cell Transplantation (HCT): CIBMTR Summary Slides, 2014. CIBMTR website. http://www.cibmtr.org.
8. Miyara M, Ito Y, Sakaguchi S. TREG-cell therapies for autoimmune rheumatic diseases. *Nat Rev Rheumatol*. 2014;10(9):543–551.
9. Finotello F, Trajanoski Z. New strategies for cancer immunotherapy: targeting regulatory T cells. *Genome Med*. 2017;9(1):10.
10. Sakaguchi S, Miyara M, Costantino CM, Hafler DA. FOXP3+ regulatory T cells in the human immune system. *Nat Rev Immunol*. 2010;10(7):490–500.
11. Dustin ML. What counts in the immunological synapse? *Mol Cell*. 2014;54(2):255–262.
12. Cullinan P, Sperling AI, Burkhardt JK. The distal pole complex: a novel membrane domain distal to the immunological synapse. *Immunol Rev*. 2002;189:111–122.
13. Zanin-Zhorov A, et al. Protein kinase C-θ mediates negative feedback on regulatory T cell function. *Science*. 2010;328(5976):372–376.
14. van Ham M, et al. TCR signalling network organization at the immunological synapses of murine regulatory T cells. *Eur J Immunol*. 2017;47(12):2043–2058.
15. Kong KF, Altman A. In and out of the bull's eye: protein kinase Cs in the immunological synapse. *Trends Immunol*. 2013;34(5):234–242.
16. Gupta S, Manicassamy S, Vasu C, Kumar A, Shang W, Sun Z. Differential requirement of PKC-θ in the development and function of natural regulatory T cells. *Mol Immunol*. 2008;46(2):213–224.
17. Zhang G, et al. In-depth quantitative proteomic analysis of de novo protein synthesis induced by brain-derived neurotrophic factor. *J Proteome Res*. 2014;13(12):5707–5714.
18. Wang X, Chuang HC, Li JP, Tan TH. Regulation of PKC-θ function by phosphorylation in T cell receptor signaling. *Front Immunol*. 2012;3:197.
19. Delgoffe GM, et al. Stability and function of regulatory T cells is maintained by a neuropilin-1-semaphorin-4a axis. *Nature*. 2013;501(7466):252–256.
20. Brunstein CG, et al. Infusion of ex vivo expanded T regulatory cells in adults transplanted with umbilical cord blood: safety profile and detection kinetics. *Blood*. 2011;117(3):1061–1070.
21. Martelli MF, et al. HLA-haploidentical transplantation with regulatory and conventional T-cell adoptive immunotherapy prevents acute leukemia relapse. *Blood*. 2014;124(4):638–644.
22. Veenstra RG, et al. B7-H3 expression in donor T cells and host cells negatively regulates acute graft-versus-host disease lethality. *Blood*. 2015;125(21):3335–3346.
23. Ferrara JL, Levine JE, Reddy P, Holler E. Graft-versus-host disease. *Lancet*. 2009;373(9674):1550–1561.
24. Schmidt A, Oberle N, Krammer PH. Molecular mechanisms of treg-mediated T cell suppression. *Front Immunol*. 2012;3:51.
25. Huang CT, et al. Role of LAG-3 in regulatory T cells. *Immunity*. 2004;21(4):503–513.
26. Merkenschlager M, von Boehmer H. PI3 kinase signalling blocks Foxp3 expression by sequestering Foxo factors. *J Exp Med*. 2010;207(7):1347–1350.
27. Xu Y, et al. IKK interacts with rictor and regulates mTORC2. *Cell Signal*. 2013;25(11):2239–2245.
28. Ma J, Ding Y, Fang X, Wang R, Sun Z. Protein kinase C-θ inhibits inducible regulatory T cell differentiation via an AKT-Foxo1/3a-dependent pathway. *J Immunol*. 2012;188(11):5337–5347.
29. Delgoffe GM, et al. The mTOR kinase differentially regulates effector and regulatory T cell lineage commitment. *Immunity*. 2009;30(6):832–844.
30. Shrestha S, Yang K, Guy C, Vogel P, Neale G, Chi H. Treg cells require the phosphatase PTEN to restrain TH1 and TFH cell responses. *Nat Immunol*. 2015;16(2):178–187.
31. Huynh A, et al. Control of PI(3) kinase in Treg cells maintains homeostasis and lineage stability. *Nat Immunol*. 2015;16(2):188–196.
32. Pollizzi KN, Powell JD. Integrating canonical and metabolic signalling programmes in the regulation of T cell responses. *Nat Rev Immunol*. 2014;14(7):435–446.
33. Buck MD, O'Sullivan D, Pearce EL. T cell metabolism drives immunity. *J Exp Med*.

2015;212(9):1345–1360.
34. Zeng H, Yang K, Cloer C, Neale G, Vogel P, Chi H. mTORC1 couples immune signals and metabolic programming to establish T(reg)-cell function. *Nature*. 2013;499(7459):485–490.
35. Byersdorfer CA, et al. Effector T cells require fatty acid metabolism during murine graft-versus-host disease. *Blood*. 2013;122(18):3230–3237.
36. Brown MJ, Hallam JA, Colucci-Guyon E, Shaw S. Rigidity of circulating lymphocytes is primarily conferred by vimentin intermediate filaments. *J Immunol*. 2001;166(11):6640–6646.
37. Burkhardt JK, Carrizosa E, Shaffer MH. The actin cytoskeleton in T cell activation. *Annu Rev Immunol*. 2008;26:233–259.
38. Roncagalli R, et al. The scaffolding function of the RLTPR protein explains its essential role for CD28 co-stimulation in mouse and human T cells. *J Exp Med*. 2016;213(11):2437–2457.
39. Liang Y, Niederstrasser H, Edwards M, Jackson CE, Cooper JA. Distinct roles for CARMIL isoforms in cell migration. *Mol Biol Cell*. 2009;20(24):5290–5305.
40. Matveeva EA, Venkova LS, Chernoivanenko IS, Minin AA. Vimentin is involved in regulation of mitochondrial motility and membrane potential by Rac1. *Biol Open*. 2015;4(10):1290–1297.
41. Nekrasova OE, et al. Vimentin intermediate filaments modulate the motility of mitochondria. *Mol Biol Cell*. 2011;22(13):2282–2289.
42. Chernoivanenko IS, Matveeva EA, Gelfand VI, Goldman RD, Minin AA. Mitochondrial membrane potential is regulated by vimentin intermediate filaments. *FASEB J*. 2015;29(3):820–827.
43. Quintana A, et al. T cell activation requires mitochondrial translocation to the immunological synapse. *Proc Natl Acad Sci U S A*. 2007;104(36):14418–14423.
44. Buck MD, et al. Mitochondrial dynamics controls T cell fate through metabolic programming. *Cell*. 2016;166(1):63–76.
45. Christie DA, Kirchhof MG, Vardhana S, Dustin ML, Madrenas J. Mitochondrial and plasma membrane pools of stomatin-like protein 2 coalesce at the immunological synapse during T cell activation. *PLoS One*. 2012;7(5):e37144.
46. Li D, Rebecca P, Cruz MA, Molldrem JJ, Champlin RE, Ma Q. Intermediate filament (IF) protein vimentin regulates T cell mediated immune response in Gvhd. *Blood*. 2015;126:3073.
47. Hsieh AC, et al. The translational landscape of mTOR signalling steers cancer initiation and metastasis. *Nature*. 2012;485(7396):55–61.
48. dos Santos G, et al. Vimentin regulates activation of the NLRP3 inflammasome. *Nat Commun*. 2015;6:6574.
49. Stevens C, et al. The intermediate filament protein, vimentin, is a regulator of NOD2 activity. *Gut*. 2013;62(5):695–707.
50. Dan HC, Antonia RJ, Baldwin AS. PI3K/Akt promotes feedforward mTORC2 activation through IKKα. *Oncotarget*. 2016;7(16):21064–21075.
51. Sarris M, Andersen KG, Randow F, Mayr L, Betz AG. Neuropilin-1 expression on regulatory T cells enhances their interactions with dendritic cells during antigen recognition. *Immunity*. 2008;28(3):402–413.
52. Liang B, et al. Regulatory T cells inhibit dendritic cells by lymphocyte activation gene-3 engagement of MHC class II. *J Immunol*. 2008;180(9):5916–5926.
53. Taylor PA, et al. L-Selectin(hi) but not the L-selectin(lo) $CD4^+25^+$ T-regulatory cells are potent inhibitors of GVHD and BM graft rejection. *Blood*. 2004;104(12):3804–3812.
54. Lin KL, et al. Intravital imaging of donor allogeneic effector and regulatory T cells with host dendritic cells during GVHD. *Blood*. 2014;123(10):1604–1614.
55. Salomon B, et al. B7/CD28 costimulation is essential for the homeostasis of the $CD4^+CD25^+$ immunoregulatory T cells that control autoimmune diabetes. *Immunity*. 2000;12(4):431–440.
56. Levine AG, Arvey A, Jin W, Rudensky AY. Continuous requirement for the TCR in regulatory T cell function. *Nat Immunol*. 2014;15(11):1070–1078.
57. Huynh A, Zhang R, Turka LA. Signals and pathways controlling regulatory T cells. *Immunol Rev*. 2014;258(1):117–131.
58. Sharma MD, et al. The PTEN pathway in Tregs is a critical driver of the suppressive tumor microenvironment. *Sci Adv*. 2015;1(10):e1500845.
59. Aoyama K, et al. Inhibiting retinoic acid signaling ameliorates graft-versus-host disease by modifying T-cell differentiation and intestinal migration. *Blood*. 2013;122(12):2125–2134.
60. Zinselmeyer BH, et al. PD-1 promotes immune exhaustion by inducing antiviral T cell motility paralysis. *J Exp Med*. 2013;210(4):757–774.
61. Zhang G, Neubert TA. Comparison of three quantitative phosphoproteomic strategies to study receptor tyrosine kinase signaling. *J Proteome Res*. 2011;10(12):5454–5462.
62. Carpén O, Dustin ML, Springer TA, Swafford JA, Beckett LA, Caulfield JP. Motility and ultrastructure of large granular lymphocytes on lipid bilayers reconstituted with adhesion receptors LFA-1, ICAM-1, and two isoforms of LFA-3. *J Cell Biol*. 1991;115(3):861–871.